

# **Statics and dynamics of granular mixtures**

## **Part 2: Dynamics**

BENJAMIN MARKS

SID: 200342291

Supervisor: Associate Professor Itai Einav

This thesis is submitted in partial fulfillment of  
the requirements for the degree of  
Bachelor of Engineering / Bachelor of Science (Honours)

School of Civil Engineering  
The University of Sydney  
Australia

27 October 2009

## Summary

Segregation, whether by income, age or language (Schelling, 1969; Traulsen and Claussen, 2004) is ubiquitous in our everyday lives. This is not merely a human trait. Any time grains are rolled down a slope (Savage and Lun, 1988; Gray and Thornton, 2005), whirled in a rotating drum (Nityanand *et al.*, 1986; Khakhar *et al.*, 1997; Khakhar *et al.*, 1999a) or shaken in a box (Knight *et al.*, 1993; Rosato *et al.*, 2002), we observe those grains organising into complex patterns. The dominant mode of segregation in granular avalanches is kinetic sieving, where separation occurs according to size (Savage and Lun, 1988; Gray and Thornton, 2005).

When looking at mechanical phenomena in general, one can begin with conservation of mass, momentum and energy. Using this tactic, many theories have been developed to help our understanding of granular avalanches, particularly those involving kinetic sieving mechanisms (Savage and Lun, 1988; Gray and Thornton, 2005). These theories are comprehensive frameworks for describing the process in mechanical terms, and give results which reflect experiment (Savage and Lun, 1988; Savage, 1987; Savage and Vallance, 2000; Bridgwater and Ingram, 1971). Our work here describes a different approach, where one ignores the mechanics of the interactions, and focuses only on the outcome of the process.

We construct a modified shear ring apparatus to simulate a granular avalanche, and use our observations of the flow to develop a simple rule which describes the segregation. We use this rule to construct a cellular automaton which crudely approximates the flow behaviour. By taking conservation of mass about this system, we define an analogous continuum theory in terms of a governing advective differential equation.

We go on to show that the two species in the flow segregate at different speeds, and quantify these relative speeds. This phenomenon has not previously been captured analytically.

## **Acknowledgements**

Firstly, I would like to thank my supervisor, Associate Professor Itai Einav, without whom I would not have had the constant guidance and expert knowledge which allowed me to accomplish this work. Secondly, I would like to thank the Particles, Grains and Complex Fluids Group at the University of Sydney, in particular Dr Pierre Rognon and Dr Bjornar Sandnes for their helpful discussions. I would also like to thank the co-author, Thomas Miller, for his invaluable help in this work. Lastly, I would like to thank the support and technical staff in the School, in particular Mr Ross Barker and Mr Sergio de Carvalho for their tireless efforts to make my experiment spin.

## CONTENTS

<b>Summary</b>	<b>ii</b>
<b>Acknowledgements</b>	<b>iii</b>
<b>Chapter 1 Introduction</b>	<b>1</b>
1.1 Statics .....	1
1.2 Dynamics .....	2
<b>Chapter 2 Literature Review</b>	<b>3</b>
2.1 Mixing flows .....	4
2.2 Brazil nut effect.....	5
2.3 Heap formation.....	6
2.4 Radial segregation .....	7
2.5 Axial banding .....	8
2.6 Kinetic Sieving .....	9
2.6.1 Savage and Lun .....	10
2.6.2 Gray and Thornton .....	12
2.7 Schelling.....	14
<b>Chapter 3 Motivation and Approach</b>	<b>16</b>
<b>Chapter 4 Research Methodology and Results</b>	<b>28</b>
4.1 Cellular automata .....	29
4.1.1 Model .....	29
4.1.2 Results .....	34
4.2 Analytic form .....	44
4.2.1 Model .....	44
4.2.2 Results .....	46
<b>Chapter 5 Summary of Results</b>	<b>49</b>

5.1 Cellular automata .....	49
5.2 Analytic model .....	49
<b>Chapter 6 Conclusion</b>	<b>50</b>
<b>References</b>	<b>51</b>
Cellular automata MATLAB© script .....	54

## Introduction

---

Granular materials exist all around us. We play with them growing up in sandboxes, we eat them in the morning as cereal and we build our houses on them. But still we know very little about them.

Consider sand on a beach. You can walk on it and it will support your weight; you can let it run through your fingers like the water in the surf, but you can not stand on the water.

Research into granular mixtures is driven largely by manufacturing. Most finished products and foods pass at some point through a granular stage — pellets of plastic, gravel in concrete, corn in a silo or powders in a pill.

“Seemingly modest changes in conditions, such as temperature, humidity, and surface conditions routinely cause earth bound devices to fail”, concluded the 2005 NASA technical report (Wilkinson *et al.*, 2005) on the importance of understanding granularity to exploring Mars and the Moon.

The report criticises industry, which in the absence of adequate granular theory relies on “millennia-long trial-and-error practices that lead to today’s massive over-design, high failure rate, and extensive incremental scaling up of industrial processes because of the inadequate predictive tools for design.”

### 1.1 Statics

Granular materials are made of small particulate matter which collectively behave as something between a solid and a liquid. Statically, the force propagation between a mixture of particles is still not well understood (Duran and Jullien, 1998; Trujillo *et al.*, 2003).

Before one can try to analyse the dynamics of a flowing situation such as inclined chute flow, one must ascertain how forces are distributed in a steady state. To do this, in Part 1 we looked at the force

propagation in a bi-disperse medium of equal sized spheres with differing elastic moduli. In Part 2 these ideas are extended into a dynamic regime.

## 1.2 Dynamics

Many different types of dynamic interaction can occur in a granular system. These include mixing, flow, vibration and fluidisation.

Mixing is one of the most important granular processes for industrial purposes. It is usually hard to mix a variety of grains uniformly (Khakhar *et al.*, 1999a). For example, suppose you try to mix granular material homogeneously using a rotating disk whose axis is horizontal. One may think that it is easy if one could continue rotation forever. Unfortunately, this is not the case even for two very similar types of grains. In fact mixing different kinds of granular matter, such as different sizes or densities, is even more difficult.

Granular matter can flow like a fluid in some cases, but does so in a remarkably different fashion from a liquid. It flows intermittently and can even get jammed, as experienced by anyone using a cheap hourglass.

Vibrating beds are becoming an attractive topic for study (Huerta and Ruiz-Suarez, 2004). Surface waves can be created in a bed of granular material, just as in a body of water (Drahn and Bridgwater, 1983). These waves are notably non-linear and behave quite differently from the analogous fluid. Under strong vibration, the bed can become fluidized and this can result in convection.

If air flows upwards into a granular bed from the bottom, the grains can act as a liquid. This kind of fluidised bed behaves very similarly to a real fluid; it even boils if enough air is pumped upwards through the system (Hoomans *et al.*, 2000). It is believed (but not yet confirmed) that a person could swim in such a bed.

## Literature Review

---

Granular materials segregate for many reasons and under many conditions. Small differences in size or density can cause the particles to segregate when flowing. While generally granular materials can be described as a continuum, and hence as fluids, there is no analogous segregative term in fluid flow.

In terms of mixing, granular materials exhibit much more complicated and varied behaviour than that of fluids (Donald and Roseman, 1962; Cleary *et al.*, 1998), and are being actively researched. For a real fluid mixture, such as salad dressing - a combination of vinegar and oil, the Navier—Stokes equations are obeyed, and so can be modelled accordingly. However for a granular flow, no such governing equation exists. Many systems have been observed which exhibit this complicated mixing, and understanding the nature of these flows is necessary for a comprehensive model of granular mixtures.

These systems come in a wide variety of forms. They can be either circular (Ottino and Khakhar, 2000) or non-circular (Khakhar *et al.*, 1999b), avalanching (Gray and Hutter, 1997; Koepe *et al.*, 1998) or continuous (Makse, 1999). Such systems may differ by density (Jain *et al.*, 2005) or size (Brone and Muzzio, 1997). In terms of how the particles interact, they may be segregating (Metcalf and Shattuck, 1996) or non-segregating (Clement *et al.*, 1995).

For such flows, there could be convection currents (Khosropour *et al.*, 1982) or even patterns (Aranson and Tsimring, 2005) forming as a result of complex flow behaviour. In this paper, we concern ourselves specifically with the pattern formation due to flow down an inclined plane (Savage and Lun, 1988; Gray and Thornton, 2005; Dolgunin *et al.*, 1998). This phenomenon has previously been studied in detail analytically, experimentally and numerically. While it is believed that the phenomenon is well understood, there are many questions with regard to the validity of the previous numerical and analytic work. This paper proceeds to take a vastly different approach to that previously considered in both the analytic and numerical work, and thus forms a new theoretical model for the phenomenon.

## 2.1 Mixing flows

A good example of a mixing flow is that occurring inside a rotating cylinder. Imagine a front loading clothes dryer full of sand. This type of flow is well defined and understood, and was investigated at length by Henein et al (Henein *et al.*, 1983). These systems are used in engineering to both separate and mix granular systems. The bed of a concrete delivery truck rotates to ensure uniform mixing, while at a slightly faster rotation speed it would separate the particles by density, as in a centrifuge.

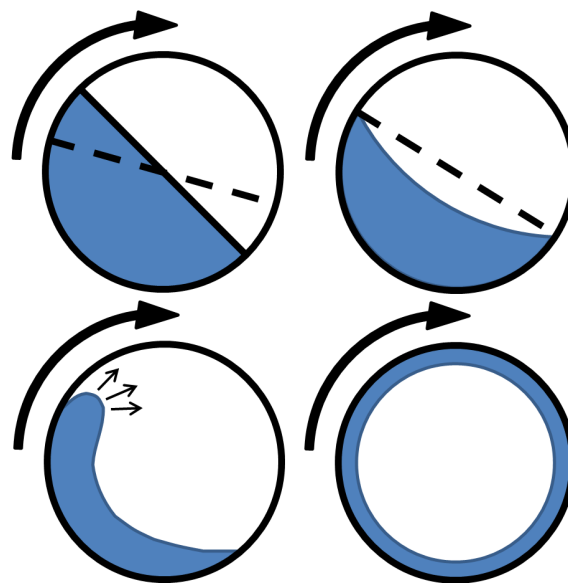


FIGURE 2.1: Mixing regimes in a rotating cylinder. Top left: Avalanching regime. Dashed line indicates slope after avalanche forms. Avalanches occur one after another, as the slope increases beyond the angle of repose. Top right: Rolling regime. Dashed line indicates angle of repose of granular material. There is a continuous avalanche of particles. Bottom left: Cataracting regime. Particles are ejected into the air. Bottom right: Centrifuging. Particles are forced outwards to the walls. The centrifugal force is now greater than the force due to gravity.

It has been shown (Henein *et al.*, 1983) that slumping and rolling are uniquely described by the rotational speed of the cylinder, the bed depth, the cylinder diameter and a few basic material properties. This group also began the use of Bed Behaviour Diagrams, a useful tool for rotating cylinder representation.

At low rotation speeds (low Froude number), the flow is characterised by individual avalanches, one after another. This is termed the avalanching regime. At higher speeds (rolling regime), a thin, rapidly flowing layer continuously flows down the free surface, which can be nearly flat. At even higher speeds,

particles begin to leave the surface (catacting regime), being propelled into the air via inertial effects. At  $Fr = 1$ , centrifuging occurs and the particles stick to the walls.

Magnetic resonance imaging, as carried out by Nakagawa (Nakagawa *et al.*, 1993) has revealed important features of the rolling regime. The free surface flow is nearly fluid-like, having a linear velocity profile across the flow, and the velocity is maximum at the middle of the flowing layer. Clement (Clement *et al.*, 1995) show similar results for a two dimensional system.

In all of these regimes, particles only flow at or near the surface. The rest of the granular material exists as a solid body and rotates with the cylinder. It is then of interest to understand what happens at the free surface, in what is known as the shear layer. This layer is the key to understanding size segregation in any flow. As a first step to understanding, we notice that segregation occurs in the shear zone, where particles at different heights move at different speeds, and hence can mix and segregate.

Many other types of segregation are evident in mixing flows, such as radial segregation and axial banding in rotating cylinders, kinetic sieving in inclined chute flow and most famously, the Brazil nut effect.

## 2.2 Brazil nut effect

When shaken, granular mixtures exhibit a particularly well publicised form of segregation. The popular scientist would have heard of the “Brazil nut effect” (Rosato *et al.*, 1986), wherein large particles rise to the top of a container of a poly-disperse mixture after prolonged vibration.

Rosato explains that the Brazil nuts rise because small nuts can squeeze into small holes and fall down, but the converse cannot occur. As a result, large particles rise through the bulk, stopping at the free surface. Another view, proposed by Knight (Knight *et al.*, 1993), shows that there is convection occurring in the pile. The downstream convection occurs in a narrow band near the edges of the container, while the center of the container rises. Because of the narrowness of the downstream convection current, large particles are excluded from passing downwards and so there is a net movement of large particles upwards.

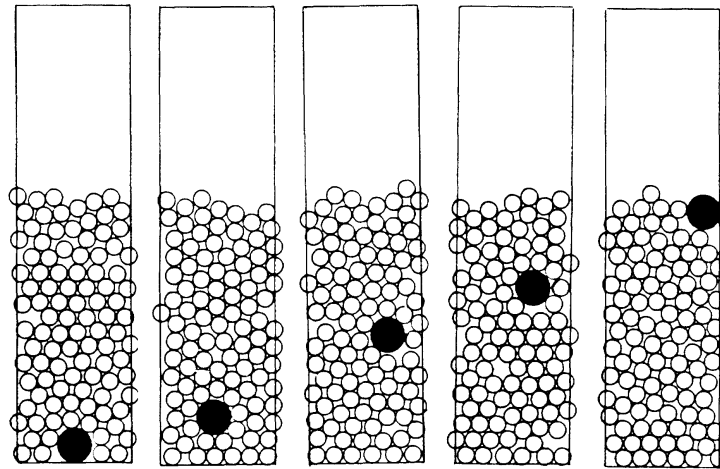


FIGURE 2.2: The Brazil nut effect, as pictured by Rosato (Rosato *et al.*, 1986). The large black particle rises to the top of the pile after the pile is shaken numerous times. The configurations were obtained after 0, 10, 30, 40 and 60 shakes (left to right). The name is used to describe a packet of mixed nuts, where the Brazil nuts (the largest of the commonly available edible nuts) are usually at the top of the packet when opened.

## 2.3 Heap formation

Segregation commonly occurs in a shear layer of a flow, such as in the case of a free flowing avalanche. For example, Drahn and Bridgwater (Drahn and Bridgwater, 1983) poured a bi-disperse mixture into a two-dimensional heap, and watched how avalanches created alternating striations of the different particles. This was further investigated quantitatively by Koepppe (Koepppe *et al.*, 1998) and explained in detail by Makse (Makse, 1997) as a combination of “spontaneous stratification” and “spontaneous segregation”. The stratification is explained as a result of the difference in angle of repose of the mixture components. Because of this difference, one component preferentially avalanches, creating layers of mono-disperse deposition. The segregation is a bulk movement of the large grains to the bottom of the pile.

This is explained again by Boutreux and de Gennes (Boutreux and De Gennes, 1996) using a coupled set of equations to describe the local density and profile defined by Bouchard et al (Bouchard *et al.*, 1994). They propose a very similar explanation, but based on a completely different analytic theory.

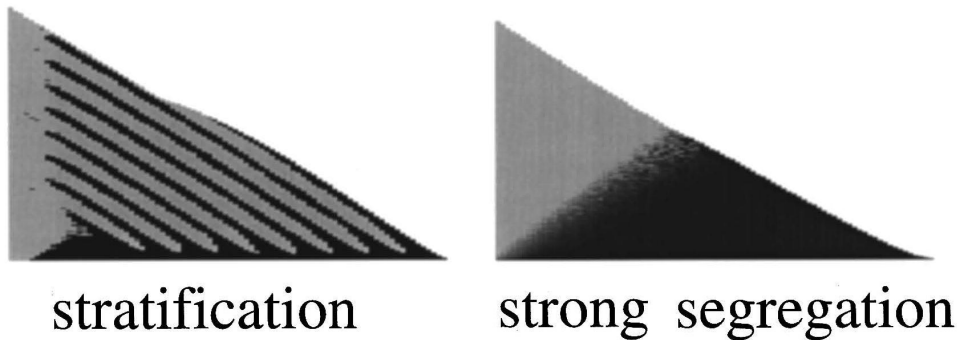


FIGURE 2.3: Steady state solutions of Makse's heap theory showing stratification and segregation as two distinct phenomena (Makse, 1997). The grey particles are larger than the black particles.

## 2.4 Radial segregation

Radial segregation is an example of shear layer segregation in circular systems. It is noted that denser or smaller particles migrate towards the inside of any curve, such as the core of a rotating cylinder. Nityanand et al (Nityanand *et al.*, 1986) conducted experimental work which showed that at low rotational speeds, percolation dominates and the small particles sink to the base, while also moving to the core, creating a pocket of small particles. Conversely, at higher speeds the opposite occurs with the small particles moving to the outside of the cylinder.

Further work has been conducted by Khakhar et al (Khakhar *et al.*, 1997) in developing a phenomenological continuum model in the flowing layer. This model is validated by both Monte Carlo and Particle Dynamics simulations. Because of the computational limits, only a small number of particles were investigated, and so close agreement between theory, experiment and simulations was not expected or achieved.

Khakhar has gone on (Khakhar *et al.*, 1999a) to investigate the dominance of chaotic advection in large systems. Most laboratory work is done on small systems, where particle diffusion is important, but scaling up to industrial sized systems requires an understanding of chaotic advection. Analytic work is compared with both computational work and experimental results. It is shown that mixing time becomes a function of the geometry of the mixing container, and the difference between circular and non-circular mixers increases with mixer size.

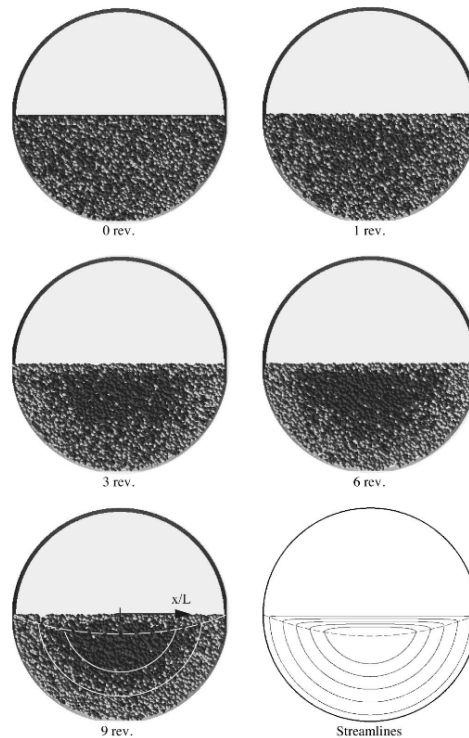


FIGURE 2.4: Time evolution of the distribution of a mixture of particles of different density, from the work by Khakhar (Khakhar *et al.*, 1997). Initially they are randomly distributed, and subsequent diagrams are after the indicated number of revolutions. Darker particles are those with higher density. Finally, the streamlines of the flow are shown.

## 2.5 Axial banding

When a rotating cylinder is placed with its axis horizontal, alternating axial bands can form due to size or density differences in particles (Donald and Roseman, 1962). This is believed to be a result of the difference in angles of repose of the mediums, which causes them to flow at different rates in the axial direction. Experimentally it has been shown (Donald and Roseman, 1962) that at large rotational speeds, axial bands form, but at low speeds mixing occurs. This is explained as a result of the angle of repose being a function of rotational speed. Because larger differences in angle of repose occur at higher speeds, more segregation occurs.

Radial segregation seems to be an important precursor to axial segregation. Yanagita (Yanagita, 1999) used a three dimensional cellular automaton to model this phenomenon and was the first to explain the

transition from radial to axial segregation. He proposed that particles slide on the surface, creating the axial segregation which is observed in experiment.

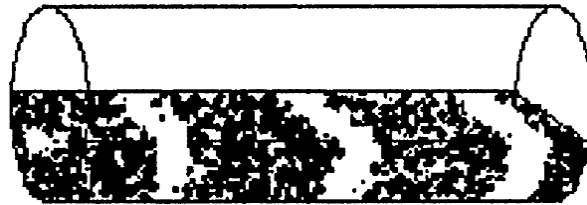


FIGURE 2.5: Sketch of axial segregation as portrayed by Yanagita (Yanagita, 1999). The black and white particles are of different sizes, and when the cylinder is rotated, segregation forms axially.

MRI imaging has been conducted by Hill (Hill *et al.*, 1997) to validate this work, and view into the bulk, not merely at the surface. The work has noted that some axially segregated regions exist in the bulk without extending to the surface. This implies that axial segregation may not in fact be driven exclusively by a surface phenomenon, as suggested by Yanagita.

## 2.6 Kinetic Sieving

Kinetic sieving is the main focus of this body of work, and is also the main form of segregation occurring in granular avalanches. Two bodies of work have been accumulated on this specific phenomenon. The first was that done by Savage and Lun (Savage and Lun, 1988), and secondly that done by Gray and Thornton (Gray and Thornton, 2005). These two approaches are wholly different, yet arrive at quite similar results (as compared in Figure 3.2). With this in mind, we can presume that there is some overarching theory which underpins both explanations. The aim of this work is to find a simple enough explanation that we can capture both theories in a comprehensive framework.

### 2.6.1 Savage and Lun

To begin, we will examine Savage and Lun's (Savage and Lun, 1988) exceptionally elegant and refined analysis. Here, two mechanisms are modelled to facilitate size segregation. The first is the "random fluctuating sieve", which is a gravity induced flow of particles into voids below them. By arranging the

flow into layers, particles which are above a vacant hole can pass down into it by free—falling under gravity. The second is “squeeze expulsion” wherein particles can become dynamically unequilibrated and be “squeezed” out from their current layer in a random direction. Squeeze expulsion was used as a mechanism to satisfy overall mass conservation and so it was deemed that its exact physical nature was unimportant.

By using a maximum entropy argument to find percolation velocities, Savage and Lun derive a continuum theory for particle size segregation in inclined chute flow. Their analytic results are then compared to experimental work done with polystyrene beads over a 1.1m chute. Two angles of inclination were tested,  $26^\circ$  and  $28^\circ$ , and for two concentrations of fines, 10% and 15%. These results were found to agree well with the analytic work, although the results obtained from the experimental work is coarse at best. Instead of mapping individual particles through the flow (which was impossible at the time), particles were collected in three bins, giving information on the vertical particle size distribution averaged over  $\frac{1}{3}$  the height of the flow. Because of the coarseness of these measurements, it is hard to show agreement or disagreement with the analytic work.

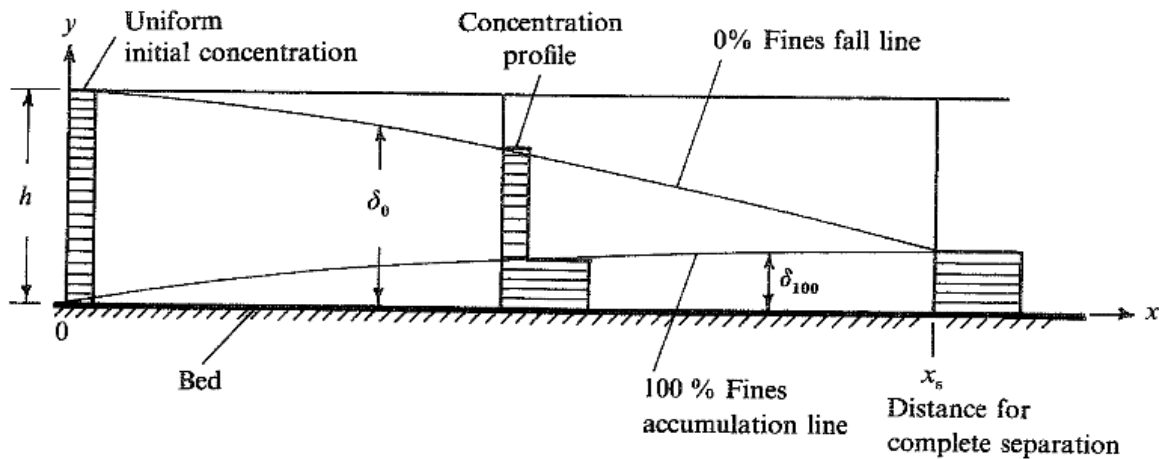


FIGURE 2.6: Concentration profiles as a function of distance as portrayed by Savage and Lun (Savage and Lun, 1988). The concentration profiles are averaged over  $\frac{1}{3}$  of the flow, giving very coarse experimental results.

The analytic work does predict a 100% fall line (a line above which no small particles are present) and a finite time for the flow to segregate fully. This seems to be in keeping with the experimental work, but the accurateness of these results is undetermined.

This model is very complex, being linked to the micromechanics of the problem, which makes it a very powerful tool for analysis. Yet with all this complexity, we are still left with the inclusion of a fitting parameter  $k_{LT}$ . The answer cannot be wholly determined from material properties alone, and must be fitted to results. If Savage and Lun went to such vast lengths to describe the flow in terms of each individual interaction between each set of particles, why should such a parameter be necessary?

### 2.6.2 Gray and Thornton

The second dominant theory explaining kinetic sieving is that proposed by Gray and Thornton (Gray and Thornton, 2005). In their paper, a binary mixture theory is used to formulate a model for kinetic sieving. The model is based on the same percolation idea, where small particles fall through available void space in the bulk, and lever large particles upwards.

The model uses conservation of mass and momentum in mixture theory to express the velocities of the components in terms of their partial densities and partial pressures. A large assumption is the fact that the percolation velocities of the components is a constant through the bulk. It is taken to be  $q^{GT} = \pm \frac{B}{c} g \cos(\zeta)$ , where  $\zeta$  is the inclination of the slope,  $c$  is the interparticle friction, and  $B$  is a dimensionless parameter. This is intended to account for varying slope, particle size, roughness and elongation. It fails to account for the interaction between particles, which is governed by the nature of the shear flow. Gray and Thornton define  $\phi$  as the small particle concentration at any point. They use  $\phi_0$  to indicate the homogeneous small particle concentration at the inlet, which is constant over the height.

A non-dimensional segregation equation is ultimately found in terms of the small particle concentration  $\phi$ , the downslope velocity  $u$ , the height  $z$ , the time  $t$  and the segregation number  $S_r$ , as follows:

$$\frac{\partial(\phi u)}{\partial t} = S_r \frac{\partial(\phi(1 - \phi))}{\partial z}$$

This equation is then solved for varying initial concentration  $\phi_0$ , varying velocity field  $u$  and segregation number  $S_r$ , a fitting parameter which defines the non-dimensional time taken to fully segregate. This analytic theory is then solved for both the time evolution of the flow and the steady state solution. Gray and Thornton require an additional assumption that there exists 3 discontinuities in  $\phi$  for all shear cases, in the form of shocks. Two of these occur at the top and bottom of the flow, and propagate towards each other through the medium. Where they meet, the third discontinuity forms, at the triple point of the flow.

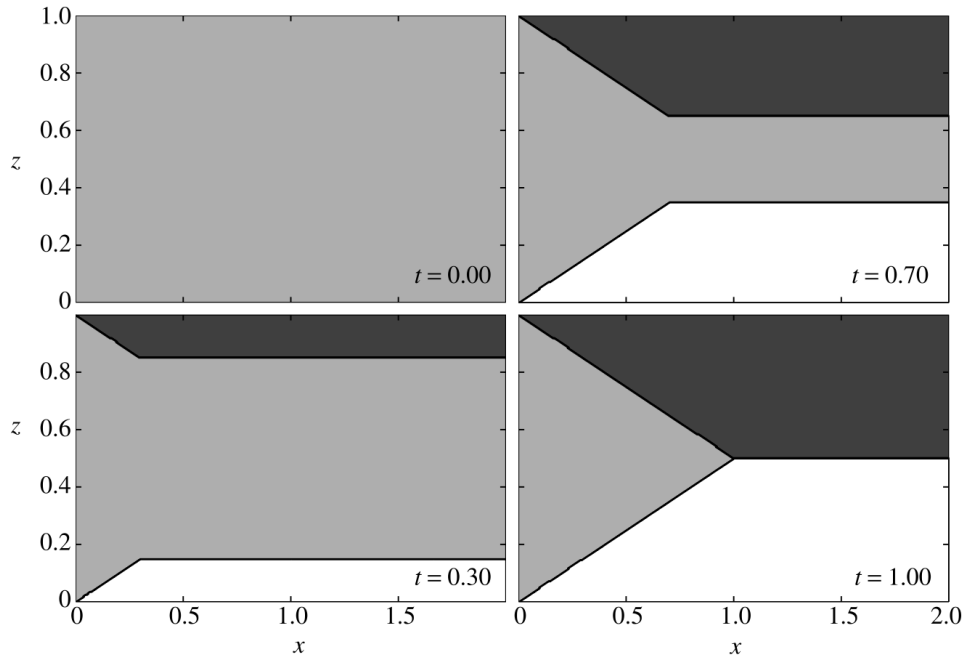


FIGURE 2.7: Time evolution of plug flow ( $u = 1$ ) with  $\phi_0 = 50\%$ . Bulk flow is from left to right. Black is  $\phi_0 = 0\%$ , gray is  $\phi_0 = 50\%$  and white is  $\phi_0 = 100\%$ . Two concentration shocks propagate towards each other over time, meeting at the triple point, where the system is fully segregated ( $x = 1, z = 0.5$ ).

From this point, two separate flows exist, that of exclusively large particles at the top, and small particles at the bottom.

A major weakness of this theory is the statement that percolation velocity is constant. This has neither been proven nor even evidenced. In fact, the competing theory of Savage and Lun proposes that the percolation velocity is a function of the shear rate,  $\frac{du}{dz}$ .

Because of this assumption, Gray and Thornton predict that segregation occurs in plug flow, as shown in Figure 2.7. Plug flow is a case where the downslope velocity is constant along the height of the flow, such as in rigid body motion. In this case there is no change in the orientation of particles with respect to one another, and so no segregation should or can occur.

Figure 2.8 implies that for different shear cases, the height of the final discontinuity should vary (looking down each column). This may be the case for compressible flows, but Gray and Thornton have explicitly stated that their model is accounting for incompressible flow only. We then ask, why would these heights change just because of the different shear regime?

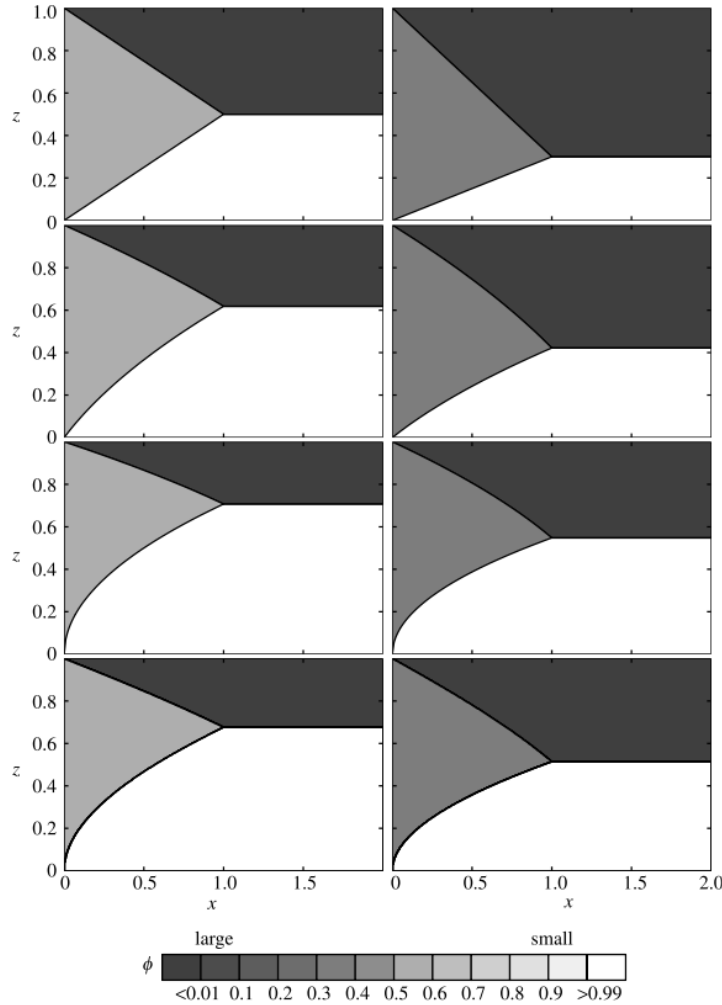


FIGURE 2.8: Gray and Thornton’s steady state solutions for four different velocity profiles and two different initial concentrations. Left:  $\phi_0 = 50\%$ . Right:  $\phi_0 = 30\%$ . Top: plug flow,  $u = 1$ . Second: basal slip,  $u = 0.5 + \frac{z}{2}$ . Third: simple shear  $u = z$ . Bottom: Bagnold velocity profile  $u = \frac{5}{3}(1 - (1 - z)^2)$ .  $S_r = 1$  for all cases, i.e. all solutions fully segregate at  $x = 1$ .

## 2.7 Schelling

We look now at a seemingly unrelated field, that of socio-economic modelling; in particular the Schelling model (Schelling, 1969), which analyses the segregation that arises from “discriminatory individual choice”. Schelling faced the daunting task of describing people’s free will and independent thought in an objective and prescriptive fashion. He described a model wherein the bulk population moved as a result of individual choices, and went so far as to describe why people moved in terms of a single rule.

People prefer to live nearby people of the same nature, be it race, sex, age or any other denomination: the driving force people feel is not to be outnumbered (Clark, 1991). They will constantly move and reshuffle until in a local majority, or some predetermined proportion. Happy people stay, unhappy people move.

Taking the analogy to granular mixtures, we have the same bi-disperse medium, with two grains of different sizes wanting to move away from one another. We can now dispense with all of the mechanics of their movements, since we know how they want to move. If they are unhappy rocks, they want to move towards their own kind. It is a very human sentiment for a rock.

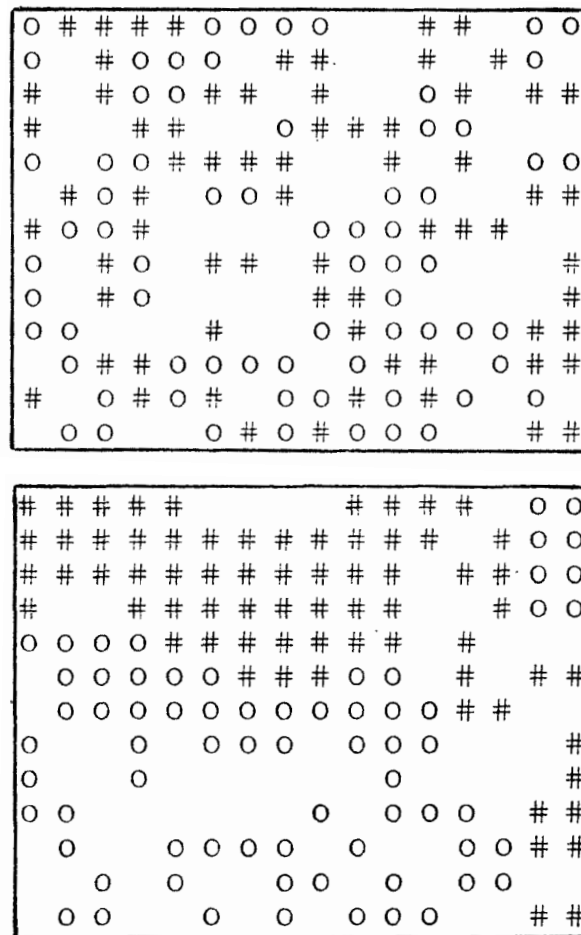


FIGURE 2.9: Top: An initial orientation of O's and #'s in Schelling's model (Schelling, 1969). Bottom: Final segregated state of O's and #'s. From an initially randomly distributed state, they have moved into regions of local majority.

## CHAPTER 3

### **Motivation and Approach**

---

There is genuinely a need for further investigation into all aspects of granular research. Avalanches pose a significant risk and area of uncertainty in both landslides and concrete production. We do not know how to design a house to resist an avalanche, nor how to pour cement and aggregate to stop them segregating before we mix them.

When a landslide occurs, we see a fast flowing region of particles moving at the free surface of the flow. Due to the chaotic and turbulent nature of the flow, there is a large degree of mixing and redistribution of particles. Because of this, we do not expect the particle size distribution to change in a predictable manner as we move downslope.

In a slightly less energetic flow, such as inclined chute flow at moderate angles (i.e.those near the friction angle of the material), we see what could be termed ‘laminar’ flow of particulate matter. In these conditions, many interesting phenomena arise. The one studied here is that of particle size segregation via kinetic sieving.

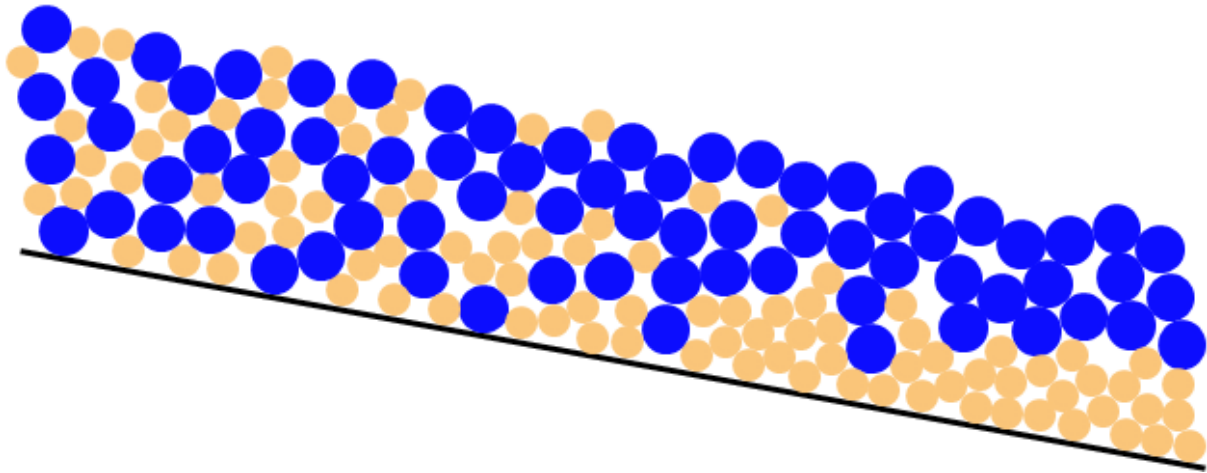


FIGURE 3.1: Effect of kinetic sieving on particles flowing down an inclined slope from left to right. At the left, the particle size distribution is constant with height, while at the right it varies with height.

When we have a mixture of two (or more) particle sizes, we find that as the flow propagates downslope, the mixture segregates into areas of uniform particle size. This comes about as a result of a mechanism known as kinetic sieving. As the particles roll down the slope, void spaces are created by the collision of the particles. Since a small particle is more likely to fit into a void than a large particle, we have a net movement of small particles downwards through the bulk, and a corresponding movement of large particles upwards. The speed of this movement is termed the percolation velocity.

The two main theories in the field of kinetic sieving are those described by Gray and Thornton (Gray and Thornton, 2005) and Savage and Lun (Savage and Lun, 1988). They both describe thin, rapidly flowing avalanches of bi-disperse mixtures down an inclined chute. Gray and Thornton use a binary mixture theory to find concentration shocks which define their solutions. Savage and Lun use a maximum entropy argument to arrive at a method-of-characteristics approach which describes a concentration profile. Each of these place significant effort into conserving momentum and energy.

Because these two theories have different forms and produce similar results, we can infer that the true behaviour of the system is some combination of the two. In the simplest possible terms, we wish to analyse both theories and find their similarities.

Often, the macroscopic behaviour of a system made up of various interacting components does not depend on the details of the interactions, but the collective behaviour (Chopard and Droz, 1998). The aggregate effect of all the microscopic interactions results in behaviour mostly related to the generic

features of microscopic interactions. The complexity of the macroscopic behaviour is disconnected from that of the microscopic, even though one is driven by the other.

With this in mind, we note that both theories include a mean segregation velocity which dictates the rate at which segregation occurs. Gray and Thornton have defined the mean segregation velocity, as  $q^{GT} = \pm \frac{B}{c} g \cos(\zeta)$ , where  $\zeta$  is the inclination of the slope,  $c$  is the interparticle friction, and  $B$  is a dimensionless parameter. Savage and Lun proposed a different, but related equation of the form  $q^{SL} = D_a \left( \frac{du}{dz} \right) (\tilde{q}_b - \tilde{q}_a)$ , where  $D_a$  is the diameter of the large particles,  $\frac{du}{dz}$  is the shear rate and  $\tilde{q}_a, \tilde{q}_b$  are the non-dimensional volume averaged velocities of the two constituents in the downslope direction.

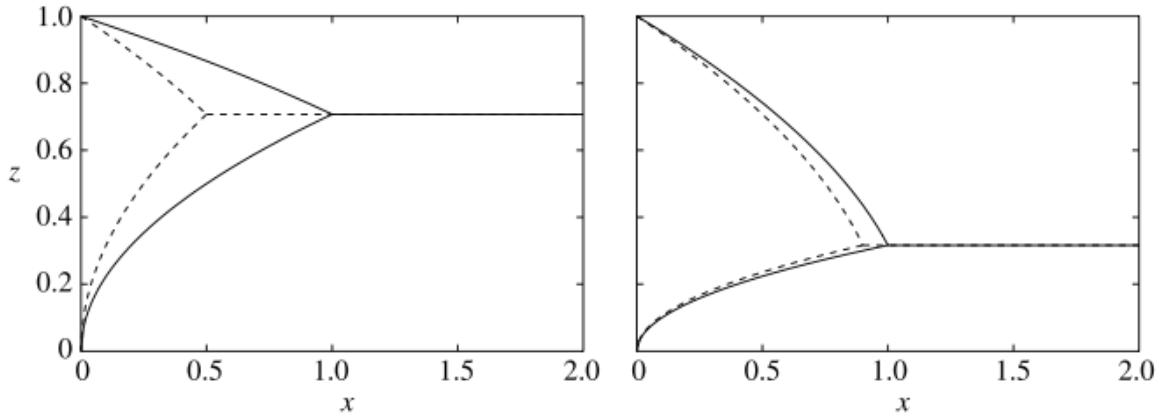


FIGURE 3.2: “The shock positions for the Savage and Lun theory (dashed line) and the current theory [Gray and Thornton] (solid line) for homogeneous inflow concentrations of 50% (left panel) and 10% (right panel) in a simple shearing flow with  $S_r = 1$ . The distances for complete segregation to occur are comparable for the dilute case, but differ significantly at larger concentrations.” (Gray and Thornton, 2005)

A comparison of the results predicted by the two theories is contained in the seminal work published by Gray and Thornton, and is included above, in Figure 3.2.

Gray and Thornton use a dimensionless parameter to indicate the specific initial conditions of the problem, the segregation number  $S_r$ :

$$S_r = \frac{qL}{UH}$$

where  $L$ ,  $H$  and  $U$  are the typical avalanche length, height and downslope velocity magnitudes respectively.

Even though many theories have been attempted to describe this work, no detailed description of the shear stresses have been successfully verified experimentally. Rognon et al (Rognon *et al.*, 2007) have defined the shear stresses using a numerical discrete element method, but the accurateness of this has not been verified in a laboratory.

We therefore know before we start, that we must attempt to verify our analytic and computational work. We choose to do this using an adaptation of the shear ring test. It consists of two stationary, concentric cylinders, and two annuli which fit between the cylinders. The lower annulus is free to rotate, and is in fact turned by a motor. The top annulus is fixed from rotating, although it can be lowered, raised and weighted.

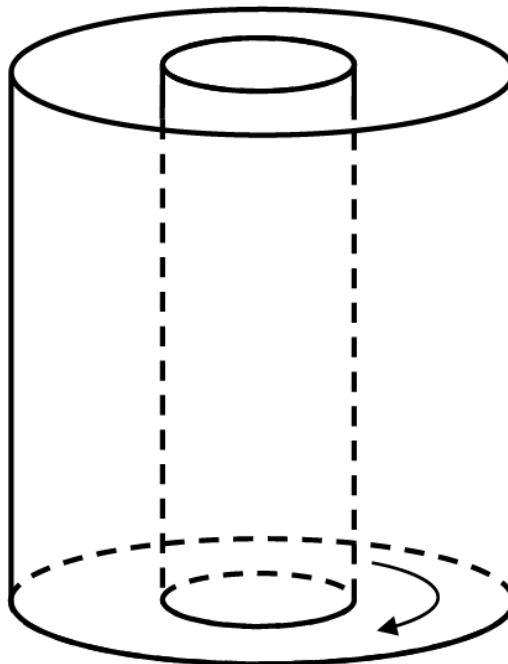


FIGURE 3.3: Experimental setup. Granular material is placed in the ring, where it is rotated to simulate avalanche flow. Optional weights can be placed on the free surface of the flow to impose loading and vary the shear case. Both walls are transparent to allow data accumulation via time lapse photography.

By placing particles between the two cylinders and the two annuli, and rotating the base annulus, shear flow is induced in the particles. A variety of shear cases can be achieved by varying the loading and the rotation speed.

As the system is circular and not linear, we expect additional shear stresses to develop in the radial direction. Radial stresses will be important when the centripetal forces are of the order of the vertical forces. We therefore set:

$$mr\omega^2 \ll mg$$
$$\omega \ll \sqrt{\frac{g}{r}}$$

For our radius of approximately 0.3m,

$$\omega \ll 5.7 \text{ rev/sec}$$

We can therefore neglect the radial shear forces for the purpose of this investigation, since we choose to operate at low angular speeds (less than  $\frac{1}{2} \text{ rev/sec}$ ).



FIGURE 3.4: The shear ring apparatus after construction. Perspex walls are mounted on a wooden frame, which holds both the shear ring and the motor.

We immediately ran into implementation problems for our setup, as the large shear ring test required a seal between the moving base plate and the rigid walls. A first iteration (outlined in Figure 3.5) was constructed but failed to adequately seal the joint. Because of this, particles were crushed in the joint and small particle fragments jammed the rotating mechanism, rapidly burning out our small motor. As a result of this, a second iteration was envisaged and constructed.

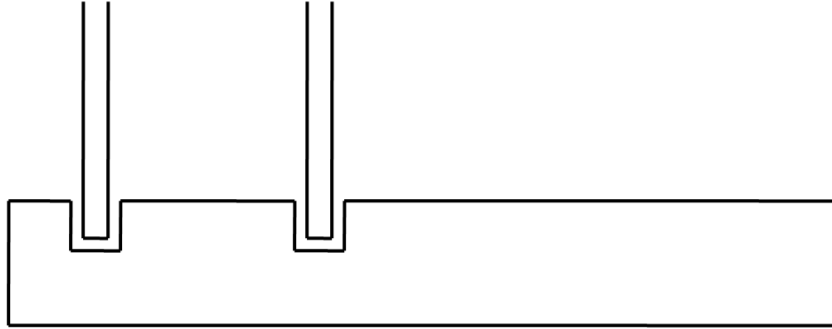


FIGURE 3.5: First choice of slip mechanism between walls and base plate. This mechanism failed to adequately keep particles out of the gaps between the walls and the base plate. This was mainly due to the large tolerances in the system because of the lack of consistent curvature in the walls.

The second iteration used perspex and metal instead of timber for the housing, and so was more stable and precise in its construction. We reduced the tolerances from 5mm to less than 2mm at the joint between the walls and the base plate, as shown in Figure 3.6. This stopped whole particles falling into the joint. We also enlarged the gap between the rotating plate and the base, allowing falling dust to pass out of the system without being trapped. This allowed us to successfully run experiments.

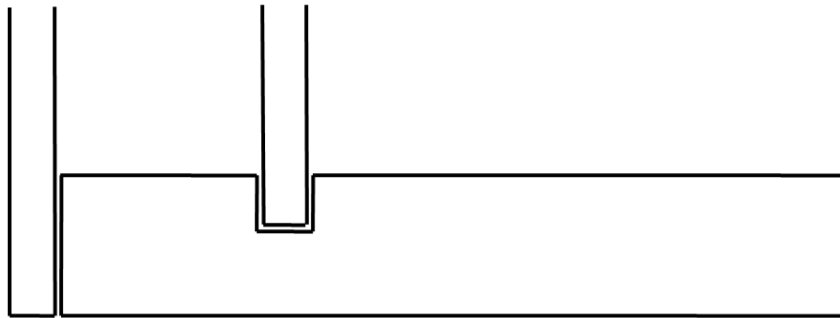


FIGURE 3.6: Second choice of slip mechanism between walls and base plate. This mechanism was adopted to keep particles out of the cavity formed at the meeting of the walls and base plate. We have significantly reduced the tolerances of the system, enabling a much closer fit between rotating base plate and stationary walls. The lack of consistent curvature of the walls was overcome by machining a round plate which is attached to the base of the outer wall. This fits with a very small tolerance ( $< 1\text{mm}$ ).

The choice of a suitable granular mixture was decided based on particle size, uniformity of particles, consistent roundness of particles and strength. We have chosen mung beans (rich green colour) as our large particles and tapioca seeds (stark white colour) as our small particles. These exhibit a diameter ratio of approximately 1.8, similar to the glass beads used successfully by Savage and Lun (Savage and Lun, 1988). Mean properties of the two particles have been obtained using a particle analyser and are outlined in the table below.

Material	CE Diameter ( <i>mm</i> )	Standard deviation ( <i>mm</i> )	Aspect ratio	Standard deviation
Mung bean	4.87	0.26	0.807	0.059
Tapioca seed	2.73	0.20	0.942	0.040

TABLE 3.1: Material properties for mung beans and tapioca seeds

CE Diameter is the circular equivalent diameter - i.e. the diameter of the circle with equivalent cross-sectional area to our particles. Aspect ratio is the maximum particle length divided by the minimum particle length in cross section. These values are all calculated by the particle analyser, for 40 mung beans and 40 tapioca seeds.



FIGURE 3.7: A mixture of mung beans (green) and tapioca seeds (white). The relative size ratio of approximately 1.5 will cause rapid segregation, and the sharp colour contrast will enable simple particle size distribution measurements by particle image velocimetry.

The choice of particles allows us to fit approximately 20 grains across the width of the apparatus. This should be sufficient to neglect edge effects at the walls and observe real avalanching at the centre of the flow.



FIGURE 3.8: A top down view of the system after segregation. Mostly green particles are visible from the top, indicating that there is a high concentration of large particles there.

Even though our particles are not entirely round or smooth, we can account for these effects in our fitting parameter  $k$ .

While at this stage we do not have a technique for finding either the particle size distributions or shear stresses experimentally, work is being done on implementing particle image velocimetry techniques using high speed cameras and post-processing to track individual particles, and infer some continuum properties.



FIGURE 3.9: A side view of the system after segregation. There are noticeably two regions of differing particle size distribution. We see small particles at the bottom, and large particles at the top.

This work aims to describe the phenomenon in its simplest terms, as described above, with a cellular automaton. Next, we wish to propose a continuum mechanical approach which is the analog of our cellular automaton. Both of these will then be compared and contrasted, and ultimately tested qualitatively against laboratory experiment, in the form of a shear ring test.

## CHAPTER 4

### **Research Methodology and Results**

---

Three distinct types of work were undertaken as part of the thesis project. Firstly, a numerical model, known as a cellular automaton, was devised and coded. This led us to an analytic form of our solution, which was modelled separately. Thirdly, both results were compared to a real world experiment using a custom made ring shear apparatus. These approaches, and their respective results, are outlined in this section.

The cellular automata is one of the simplest types of numerical simulation. For this reason, it is used to model highly dynamic situations. By creating a simple system that behaves in a complicated manner, we feel that our assumptions in creating the cellular automata reflect quite accurately what is occurring in the physical system.

What we have found, in fact, is that our cellular automata predicts not only the global behaviour of the system, but gives us an insight into the mechanics of the interactions between the particles.

## 4.1 Cellular automata

### 4.1.1 Model

The cellular automata defined here works in a regular 1 dimensional lattice, where the diameter of each particle,  $d_i$ , is a Boolean variable attached to each site  $i$  of the lattice. The model ignores physical size differences between particles, as well as all other physical properties. We then define a single rule which specifies the time evolution of the diameter at each site.

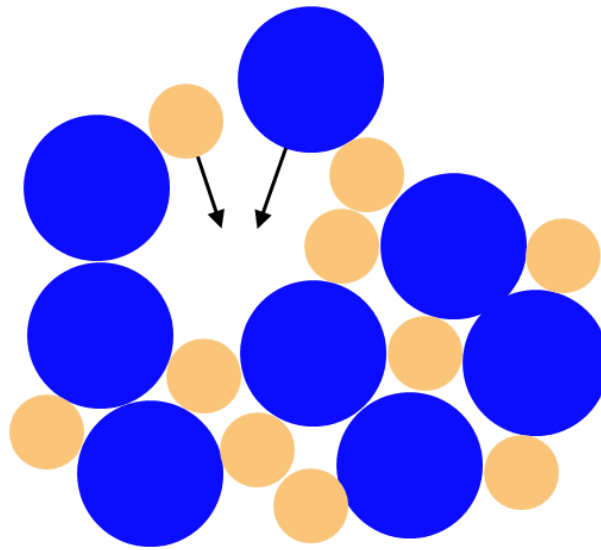


FIGURE 4.1: Orange are small particles, Blue are large particles. Two particles attempting to fall into an available space. The small particle is more likely to fit into any given void, and so we have a net movement of small particles downwards, and a corresponding movement of large particles upwards.

In Figure 4.1, either of the two particles indicated could fall into the available space. We find that the smaller particle is more likely to fit in the void, and so this has a greater probability of falling. This can be expressed in simplest terms in one dimension as two particles swapping places. We then describe our rule as the following; with some frequency  $f$

$$d_i \Leftrightarrow d_{i-1} \text{ if } d_i < d_{i-1}$$

Figure 4.2, below, illustrates two iterations of the rule on a three particle system. In both cases, the small particles swap with the larger particles, creating segregation. We run our simulation simultaneously in

many instances, and average the particle diameter at each point across these simulations, as shown in Figure 4.3. By compiling the data across all time steps, we gain a picture of the flow moving downslope.

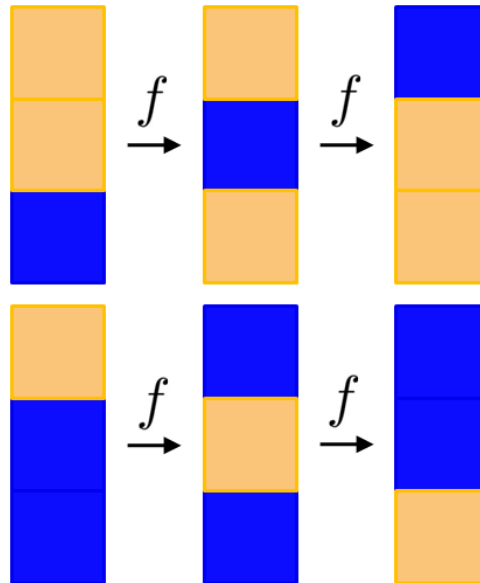


FIGURE 4.2: Orange are small particles, Blue are large particles. The automata mechanism, where large and small particles swap places with frequency  $f$ . Three iterations of this mechanism are shown, for two different initial configurations. In both cases, the small particles end up on the bottom of the pile.

This can be done for varying frequency of swapping, small particle concentration and even for poly-disperse flows.

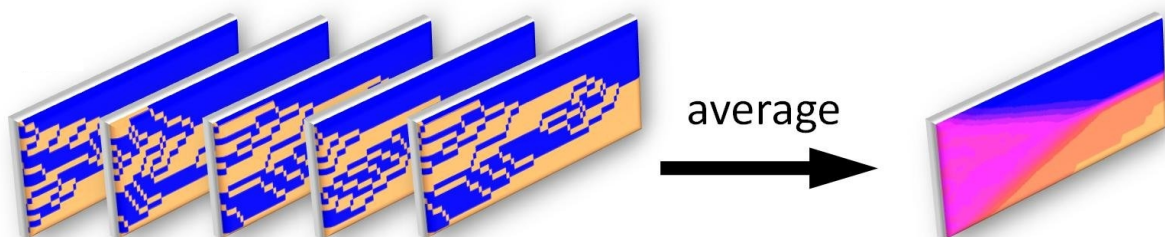


FIGURE 4.3: Orange are small particles, Blue are large particles. Individual simulations are averaged to produce mean model behaviour.

The mean diameter at any point is defined as the average diameter of all particles into the page at the same height. If a particle is larger than the mean diameter at any point, it swaps with a neighbour below, i.e.  $d_i \Leftrightarrow d_{i-1}$  if  $d > d_i$ . The code was written in MATLAB<sup>®</sup> and is attached in Appendix 1. It is explained diagrammatically in Figure 4.4.

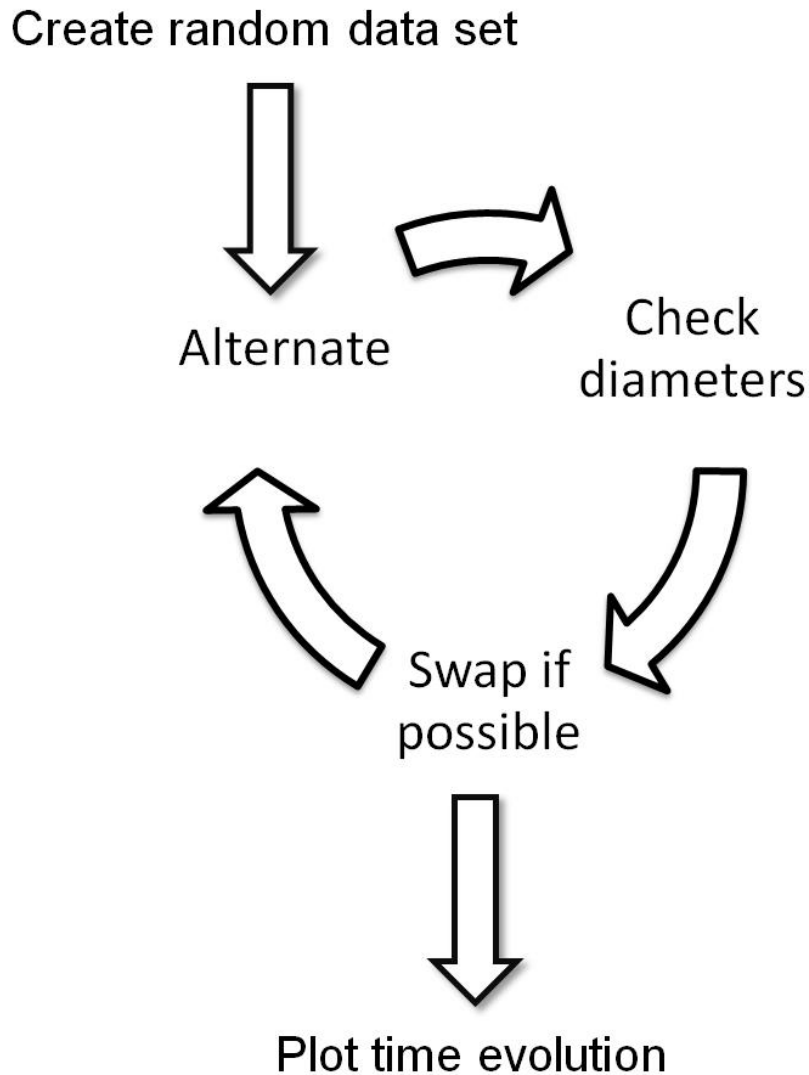


FIGURE 4.4: Flow chart describing the cellular automata code. An initial random configuration of particles is processed such that the mechanism outlined above occurs. After a sufficiently long time, the time evolution of the flow is outputted.

We begin with an initially randomised set of nodes in two dimensions, with each having a discrete particle at the node. The diameter of the particle at each node can be either big (0) or small (1). The two dimensional lattice represents many one dimensional simulations running simultaneously. The data is randomised such that the average in both directions of the matrix is equal for every row and column. We call this  $\phi_0$ , the initial concentration of small particles.

Initial particle randomness is ensured both along the height and into the bulk simultaneously by randomly filling an empty matrix with the required number of particles in every row and column, much

like a binary sudoku, where the sum of each row and column is fixed. This method of random filling has its drawbacks, however, as there is often not a unique solution for large matrices. This hindrance is counteracted by constructing large matrices from a superposition of randomly generated smaller matrices. While this ensures that the required concentrations are correct, it also adds a second scale of randomness to the matrix. This is not ideal, but is sufficient for the purposes of this experiment and provides optimal randomness in a minimal amount of computational time.

For each timestep, we then check every node. If the node is above a layer of larger average particle diameter, it has a probability of swapping with the particle directly below it, as defined by our frequency  $f$ . For stability, we iterate in half time steps, such that odd columns are processed separately, before even columns.

After the system has fully segregated, or at some given time, the time loop stops and a contour plot of the time evolution is outputted.

The behaviour of the system is determined largely by our parameter  $f$ . We have obtained this by extending Gray and Thornton's segregation number  $S_r$  so that the tendency for our mechanism to occur is a function such that  $f \propto \frac{q^{SL}}{U} \propto \frac{du}{dz}$  where  $\frac{du}{dz}$  is the shear rate. We can choose a variety of flows to model, each with their own shear rate. They are summarised in the following table.

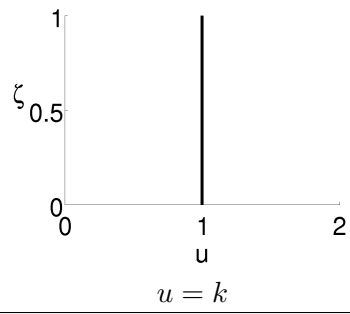
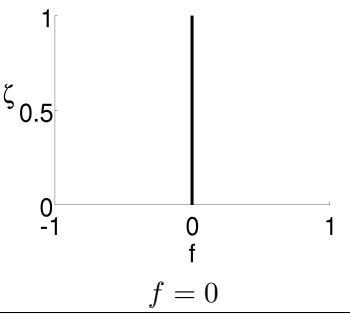
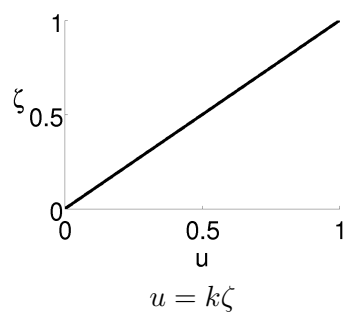
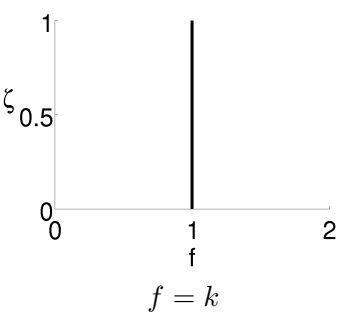
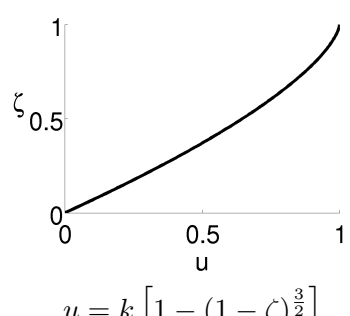
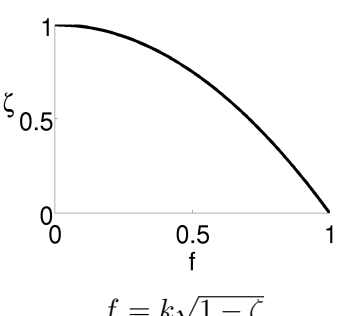
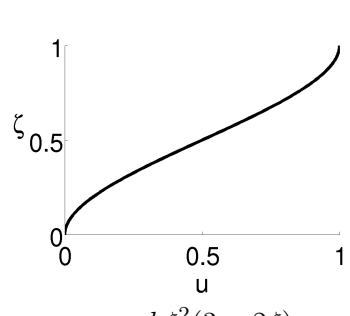
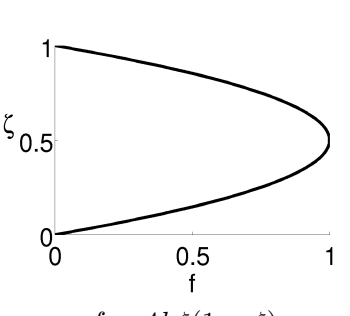
Flow regime	$u$	$f$
Plug flow	 <p style="text-align: center;"><math>u = k</math></p>	 <p style="text-align: center;"><math>f = 0</math></p>
Simple shear	 <p style="text-align: center;"><math>u = k\zeta</math></p>	 <p style="text-align: center;"><math>f = k</math></p>
Bagnold shear	 <p style="text-align: center;"><math>u = k \left[ 1 - (1 - \zeta)^{\frac{3}{2}} \right]</math></p>	 <p style="text-align: center;"><math>f = k\sqrt{1 - \zeta}</math></p>
Shear band flow	 <p style="text-align: center;"><math>u = k\zeta^2(3 - 2\zeta)</math></p>	 <p style="text-align: center;"><math>f = 4k\zeta(1 - \zeta)</math></p>

TABLE 4.1: Shear flow regimes. Four shear flow regimes discussed in this paper, namely plug flow, simple shear, Bagnold shear and shear band flow.

These four shear flows correspond to different physical flows. Plug flow is that observed when a pile of grains is moved without disturbing the internal structure, i.e. rigid body motion. For this case, obviously, we expect no segregation. The second case is simple shear, the simplest model for a sheared flow. We assume zero velocity at the base of the flow, and free flowing at the free surface. We linearly interpolate between these two points to describe the velocity profile and the shear strain profile. A more accurate representation of particle flow is that proposed by Bagnold (MiDi, 2004; Silbert *et al.*, 2001). This velocity profile assumes mono-disperse particle flow, and has been extended by Rognon (Rognon *et al.*, 2007) for bi-disperse flows.

The constant  $k$  is itself a function of  $\frac{B}{c}g \cos(\zeta)$ , as described by Gray and Thornton. This includes all of the contributions due to particle sizes, roughness and circularity.

This theory predicts that the solution will evolve towards a simple limit point in the phase space, ie that all initial configurations will propagate towards a similar steady solution. Many cellular automata (Wolfram, 1986; Chopard and Droz, 1998) are known to exhibit such behaviour, and the design of a cellular automaton that models the correct results implies that the essential aspects of the complex phenomena have been recognised and reduced to a simple form.

### Non-dimensionality

We define a non-dimensional height  $\zeta$  such that  $\zeta = \frac{z}{H}$ , where  $H$  is the avalanche depth. In our model,  $\zeta = \frac{i}{N}$  where  $N$  is the total number of nodes in the vertical direction and  $i$  is the current node. We also define a non-dimensional time  $\tau = j \frac{k}{N} = t \frac{kU}{H}$ . The first equality refers to the cellular automata, where  $j$  is the timestep. The second equality refers to the physical time  $t$ , where  $U$  is the average bulk velocity across the depth and  $H$  is the avalanche height.

The flow is described by  $\phi$ , the small particle concentration. We find  $\phi$  by summing the number of small particles at a given height across all of the simulations, and dividing by the total number of simulations.

#### 4.1.2 Results

The cellular automata outputs a contour plot of the time evolution of  $\phi$  for any applied shear regime and initial concentration of  $\phi$ . Figure 4.5 outlines the case of Bagnold shear, with initial concentration of 32%. Because of the large percolation frequencies at the base of the flow, we see a concentration shock - a discontinuity in the small particle concentration. At the top of the flow, however, the percolation

frequency is uniquely zero, and a second concentration shock does not develop. In this case, there is no robust definition of complete segregation. In a flow of infinite width, segregation would never fully occur.

#### 4.1.2.1 Overview

To understand the results outputted by the cellular automata, we must begin by discussing the shear flow in question. Figure 4.5A shows a Bagnold shear flow, with the velocity field given by  $u = 1 - (1 - \zeta)^{\frac{3}{2}}$ . This implies that the percolation frequency,  $f$  is near zero at the top, and large at bottom, as shown in Figure 4.5B. This means that we expect rapid segregation at the bottom of the flow, and only slow segregation at the top. We therefore do not expect a concentration shock at the top of the flow.

While we do not expect a concentration shock, we expect that in a situation such as described by Savage and Lun, with a small number of particles (they have a flow of 10-20 particles deep) there would be a well defined line above which no particles exist. This line would then correspond to the lower bound of the bluest region contained in our results, which behaves in a similar fashion to that described by Savage and Lun.

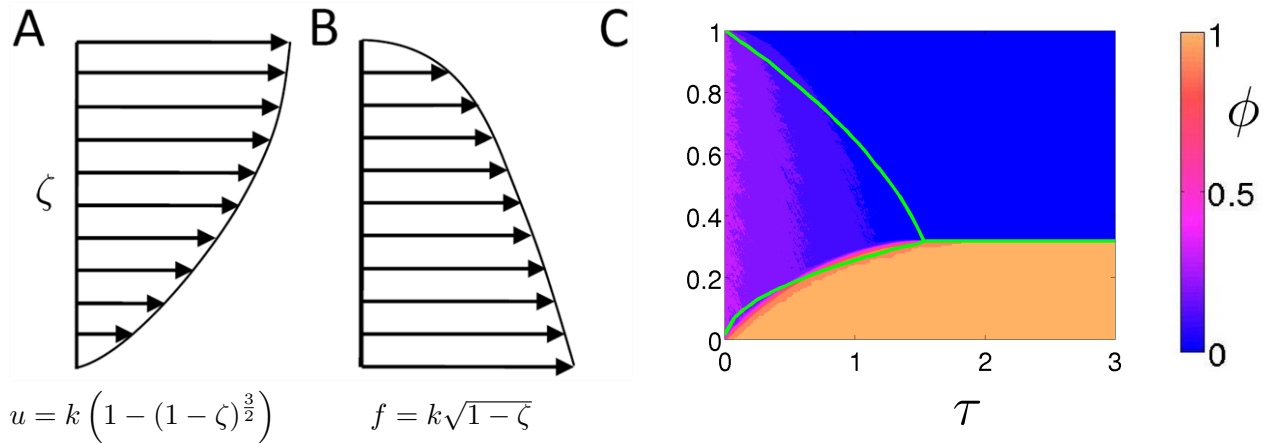


FIGURE 4.5: A: Bagnold velocity profile. B: Percolation frequency distribution. C: Steady state solution for a Bagnold shear case. Bulk flow is from left to right. The chute is initially filled with a mixture of 32% small concentration. At the inlet, more of the mixture enters the chute and flows downslope. Colours represent small particle concentration  $\phi$ . Green lines are experimental results of Savage and Lun (Savage and Lun, 1988) as displayed by Gray and Thornton (Gray and Thornton, 2005).

Figure 4.5 has an overlay of the analytic work done by Savage and Lun, as pictured in (Gray and Thornton, 2005). In this work, the concentration was described in terms of volume. This has been

converted from the stated 10% small concentration by volume, to 32% concentration by particle number for the purposes of the comparison.

#### 4.1.2.2 Plug flow

For the simplest case of particle flow, we model plug flow. Gray and Thornton expect segregation to occur for this regime (as pictured in Figures 2.7 and 2.8). Plug flow describes a flow which does not change while propagating. From the perspective of any given particle, its neighbours would not move relative to itself as it flowed downslope - imagine a bucket of particles being picked up and moved without disturbing the contents. Obviously, we do not expect to observe segregation in this regime. Because Gray and Thornton have neglected the role of the shear interaction of the particles as a precursor for segregation, they expect segregation where it is evident that there should be none.

#### 4.1.2.3 Simple shear

Figure 4.6 represents the time evolution of simple shear flow. We note that this is described by  $f_1 = k_1$ , i.e. the frequency is constant along the height. It is evident that the same results are found as those predicted by Gray and Thornton for the plug flow case, and our analytic solution matches theirs for this case only. The characteristics are linear, and the concentration shocks move towards a triple point at fixed speed.

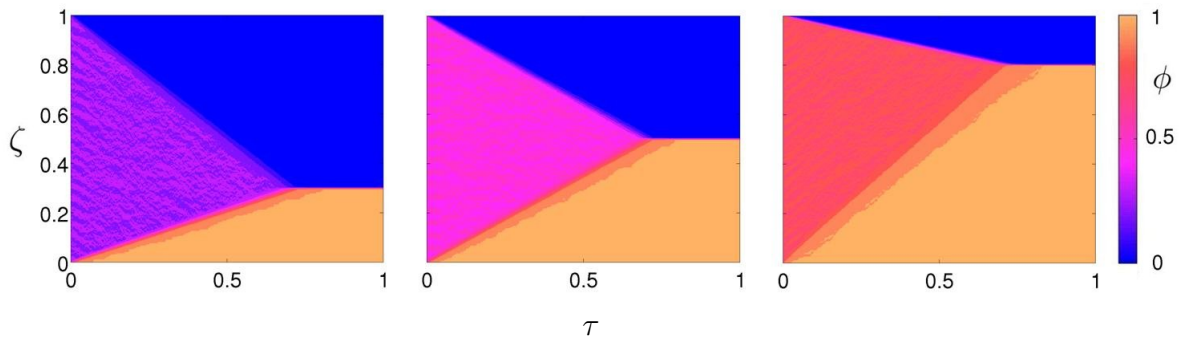


FIGURE 4.6: Time evolution for simple shear flow, i.e.  $f_1 = k$ . Bulk flow is from left to right. The chute is initially filled with a mixture of 30%, 50% and 80% (left to right) small concentration. At the inlet, more of the mixture enters the chute and flows downslope. Colourbar represents small particle concentration  $\phi$ .

The position of this triple point along the slope is varied by changing  $k_1$ , and the position above the base of the avalanche is varied by changing  $\phi$ .

#### 4.1.2.4 Linear shear

A more realistic case is that of a linear shear profile, as shown in Figure 4.7. Here we see only one concentration shock, at the bottom of the flow. Again, full segregation takes an infinite time to occur.

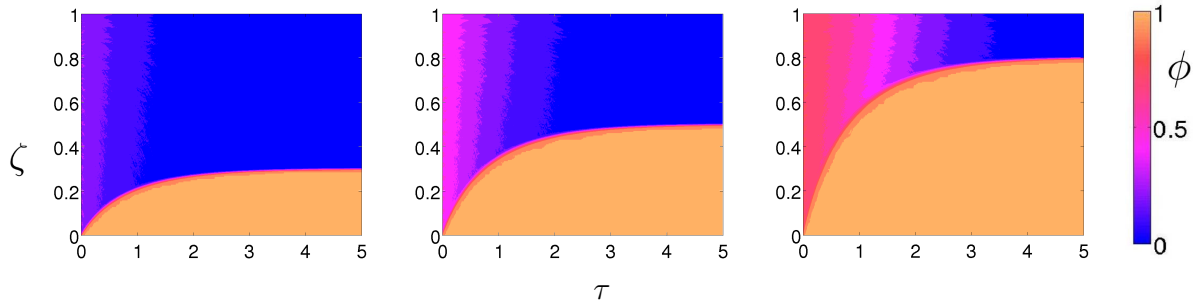


FIGURE 4.7: Time evolution for linear shear flow, ie  $f = k(1 - \zeta)$ . Bulk flow is from left to right. The chute is initially filled with a mixture of 30%, 50% and 80% (left to right) small concentration. At the inlet, more of the mixture enters the chute and flows downslope. Colourbar represents small particle concentration  $\phi$ .

#### 4.1.2.5 Shear band flow

Shear band flow presents an interesting case as pictured in Figure 4.8. Here, concentration shocks develop at neither the top nor the bottom. There is, however a sharp concentration shock which develops rapidly at the near fully developed state. Again, segregation never fully occurs.

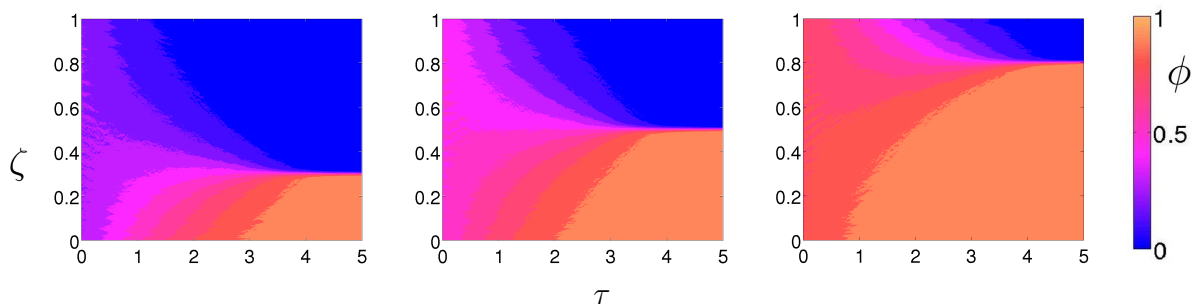


FIGURE 4.8: Time evolution for shear band flow, ie  $f = k\zeta(1 - \zeta)$ . Bulk flow is from left to right. The chute is initially filled with a mixture of 30%, 50% and 80% (left to right) small concentration. At the inlet, more of the mixture enters the chute and flows downslope. Colourbar represents small particle concentration  $\phi$ .

### 4.1.2.6 Bagnold shear

Bagnold shear is an accurate model for flow of mono-disperse spheres down an inclined plane. As compared with the results of Savage and Lun (Figure 4.5), this model presents a realistic and appropriate choice for our model of real-world behaviour. A concentration shock builds at the bottom of the flow only. This is shown for three initial concentrations of  $\phi$  in Figure 4.9 below.

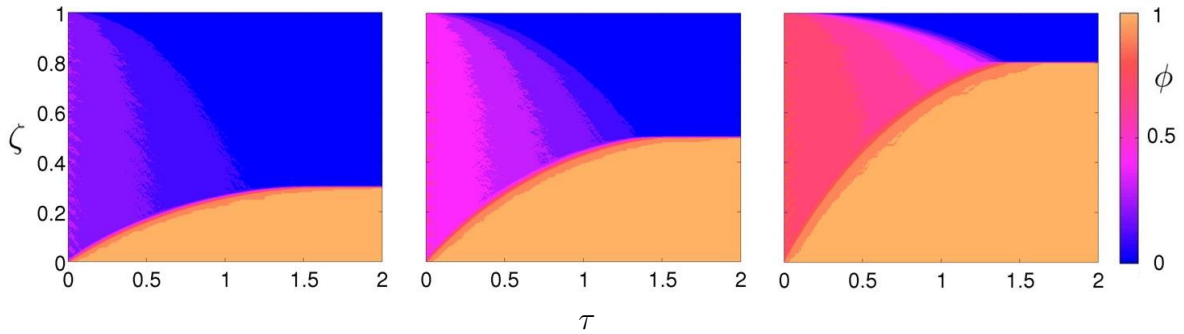


FIGURE 4.9: Time evolution for Bagnold shear, i.e.  $f_2 = k\sqrt{1-\zeta}$ . Bulk flow is from left to right. The chute is initially filled with a mixture of 30%, 50% and 80% (left to right) small concentration. At the inlet, more of the mixture enters the chute and flows downslope. Colourbar represents small particle concentration  $\phi$ .

While this regime is a good approximation for a mono-disperse medium, it does not account for the bi-disperse flow. To accurately account for this, we could use the shear rate defined by Rognon et al (Rognon *et al.*, 2007). This shear rate, however, has not yet been implemented in our model, due to the additional complexity.

### 4.1.2.7 Concentration shocks

We note in Figure 4.10 that for the simple shear case, there exists a sharp discontinuity, or shock, at both the top and bottom boundaries (left side). Quite distinctly differently we note that on the right hand side, there is only a shock at the bottom of the flow, and we have a continuous surface describing our concentration profile. This is a major difference between our theory and both previous theories, and we explain it as a result of the low shear at the top of the flow, where we expect very little segregation due to kinetic sieving. Experimentally, it has been observed that particles jostle and in fact fly over each other at the free surface, but we consider this to be a separate effect from that of kinetic sieving. This phenomenon is known as cataraction.

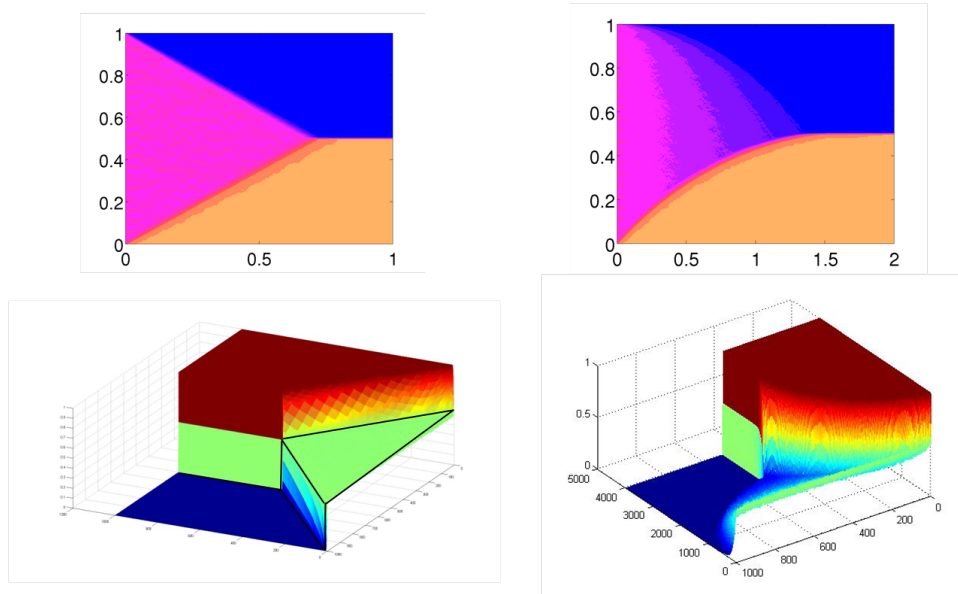


FIGURE 4.10: A comparison of two cases, both with initial concentrations of 50%. Left: Simple shear. Right: Bagnold shear. The bottom figures are 3D surface plots of the same data, showing the sharp discontinuities at joints between regions. All joints between areas are shocks except the top of the Bagnold shear case, where the solution is continuous.

#### 4.1.2.8 Size discrimination

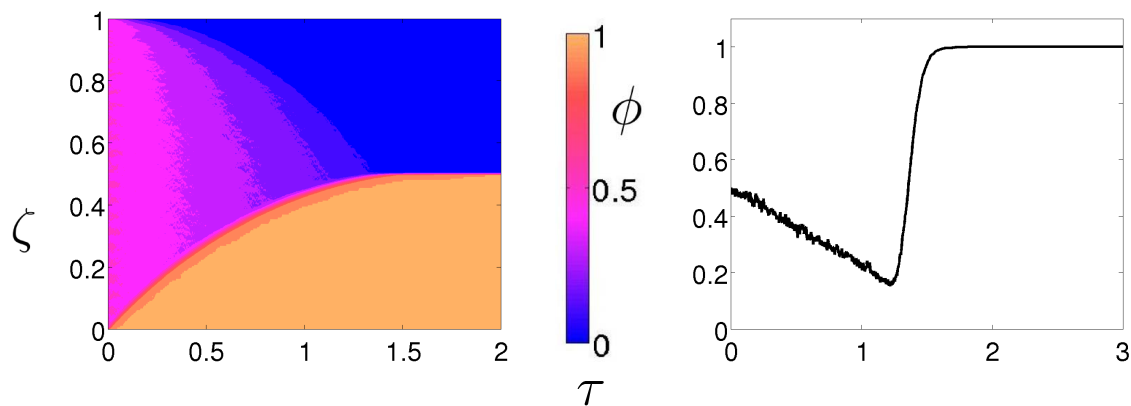


FIGURE 4.11: Left: Time evolution for Bagnold shear with initial concentration of 50%. Right: A slice through the plot at left at  $\zeta = 0.5$ .

Revisiting a previous case, that of homogeneous Bagnold shear, we note that at mid-height in the flow, at  $\zeta = 0.5$ , the small particle concentration drops before returning to its initial value, as in Figure 4.11 (left). The right hand side of this Figure is a slice through the plot at left, at  $\zeta = 0.5$ . It shows that there

are significantly less small particles present during the intermediate stage before full segregation. We can then ask ourselves the following:

Are the large particles moving faster than the small ones? How else did they get here from the bottom before small ones got here from the top?

We now look at a different case, that of heterogeneous initial conditions. By placing a small amount of large (or small) particles at the top (or bottom) of the flow, we can get an understanding of how rapidly these two species flow past one another. This is pictured in Figure 4.12. The top two Figures picture large particles moving upwards through the bulk (left), and small particles moving downwards (right), in separate simulations. For each case, we use two homogeneous regions of pure small and large particles, and size the regions in the ratio 1:9.

The bottom graph represents a competition between the two simulations. We place a 'gate' at some height  $d$ , and time until 90% of the contaminant particles have passed beyond this gate. We have plotted this time for a range of values of  $d$  for both simulations. We note that for any distance moved by the particles, the small particles (yellow line) take longer to reach the gate. This proves that the large particles are in fact faster than the small particles!

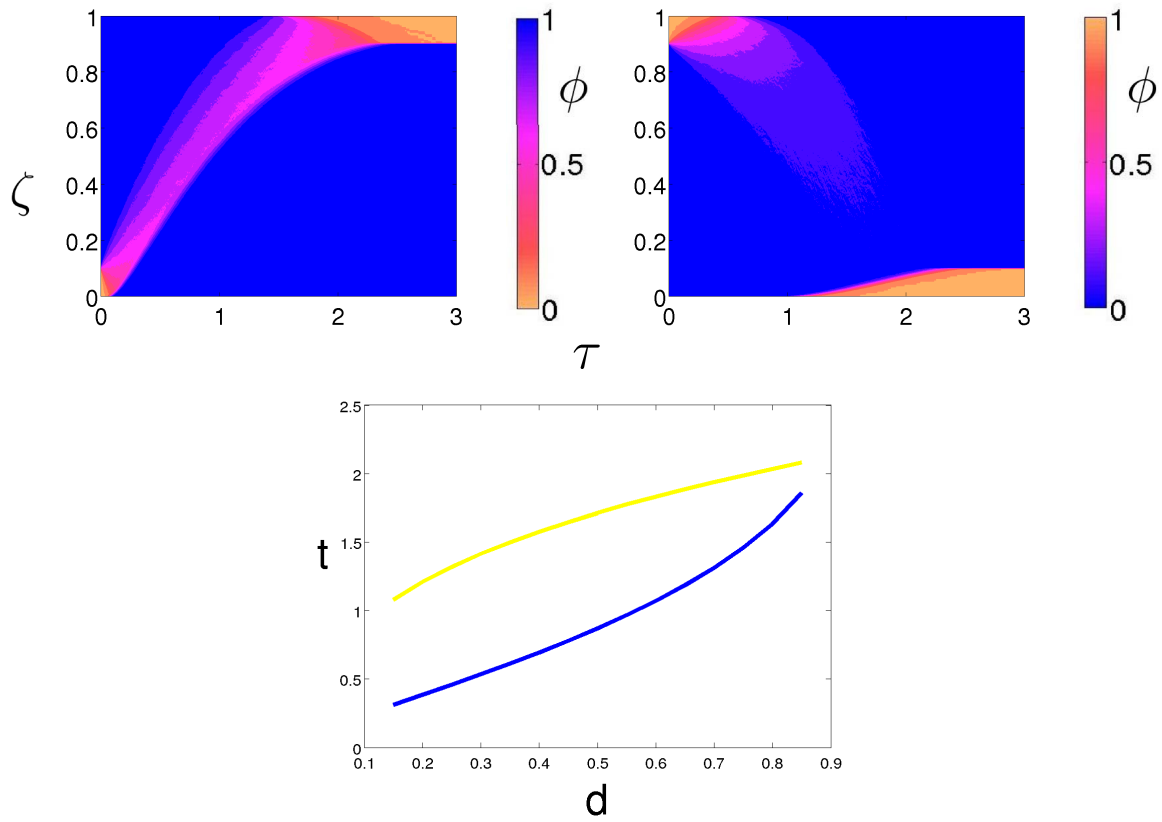


FIGURE 4.12: Top left: Large particles rising to the top of the flow, under Bagnold shear. Top right: Small particles sinking to the bottom of the flow, under Bagnold shear. Bottom: The time for 90% segregation at a particular height  $d$ . The blue line is large particles moving upwards, and the yellow line is small particles moving downwards.

## 4.2 Analytic form

### 4.2.1 Model

By taking conservation of mass about a single node, we can show that this cellular automata approach can be reduced at a continuum model, comparable to that of Gray and Thornton. We begin with the fluxes present at a single node, as shown below.

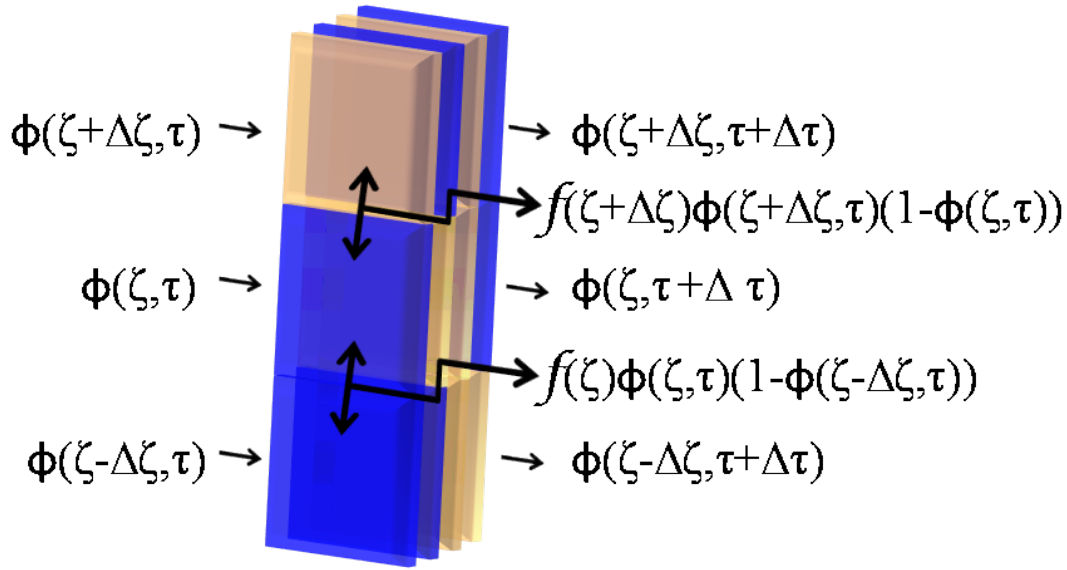


FIGURE 4.13: Fluxes of small concentration at a node. We take conservation of mass about this point to define our continuum theory.

For this process we use non-dimensional units as defined previously. Here  $\phi$  is the small particle concentration,  $u$  is the downslope velocity,  $\zeta$  is the height and  $\tau$  is the time. Taking conservation of mass:

$$\phi(\zeta, \tau)\Delta\zeta + f(\zeta + \Delta\zeta)\phi(\zeta + \Delta\zeta, \tau)(1 - \phi(\zeta, \tau))\Delta\tau - f(\zeta)\phi(\zeta, \tau)(1 - \phi(\zeta - \Delta\zeta, \tau))\Delta\tau = \phi(\zeta, \tau + \Delta\tau)\Delta\zeta$$

Which reduces to:

$$\frac{\partial\phi}{\partial\tau} = \frac{\partial(f\phi)}{\partial\zeta} - \frac{\partial(f\phi^2)}{\partial\zeta}$$

Or alternatively,

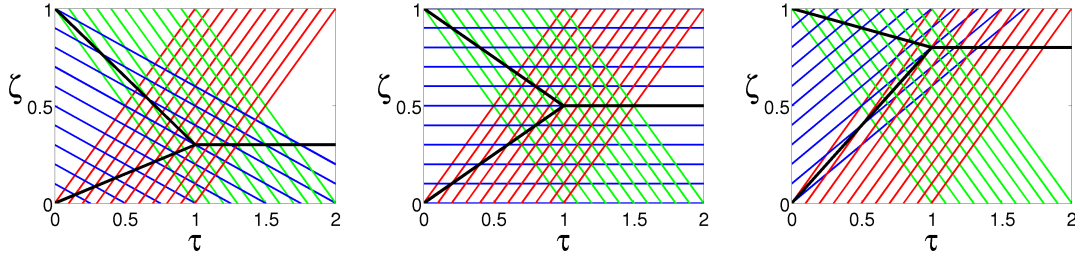


FIGURE 4.14: Concentration shocks developing in three steady state solutions. All have  $k = 1$ . From left to right:  $\phi_0 = 30\%$ ,  $\phi_0 = 50\%$  and  $\phi_0 = 80\%$ . The shocks split the domain in three areas, split by the black lines. The top area contains only small particles, the bottom only large particles and the region on the left contains a uniform mixture of the two, at the initial concentration.

$$\frac{\partial \phi}{\partial \tau} = \frac{\partial (f\phi(1 - \phi))}{\partial \zeta}$$

For simple plug flow cases, we can take  $f = k$  to be a constant with depth,  $\zeta$ . Our solution now reduces to that of Gray and Thornton. An analytic solution is now available by use of the method of characteristics, as shown in Figure 4.14. By solving for the known concentration shocks, we have again shown linear concentration shocks in the system. The position of the shock varies with  $k_1$  and initial concentration  $\phi_0$ .

With reference to the analytic form proposed by Gray and Thornton,

$$\frac{\partial(\phi u)}{\partial \tau} = S_r \frac{\partial(\phi(1 - \phi))}{\partial \zeta}$$

we see that our cellular system neglects the variation of downslope velocity with height. Our cellular automata has functioned in a Lagrangian space, i.e. we have neglected the downslope velocities due to the limits of the simplistic approach. In our analytic form, however, we are free to add such a rule. By now including this in the system, we get the following conservation form, as shown in Figure 4.15.

This modifies our conservation equations to become:

$$\frac{\partial(\phi u)}{\partial \tau} = \frac{\partial(f\phi(1 - \phi))}{\partial \zeta}$$

which reduces to

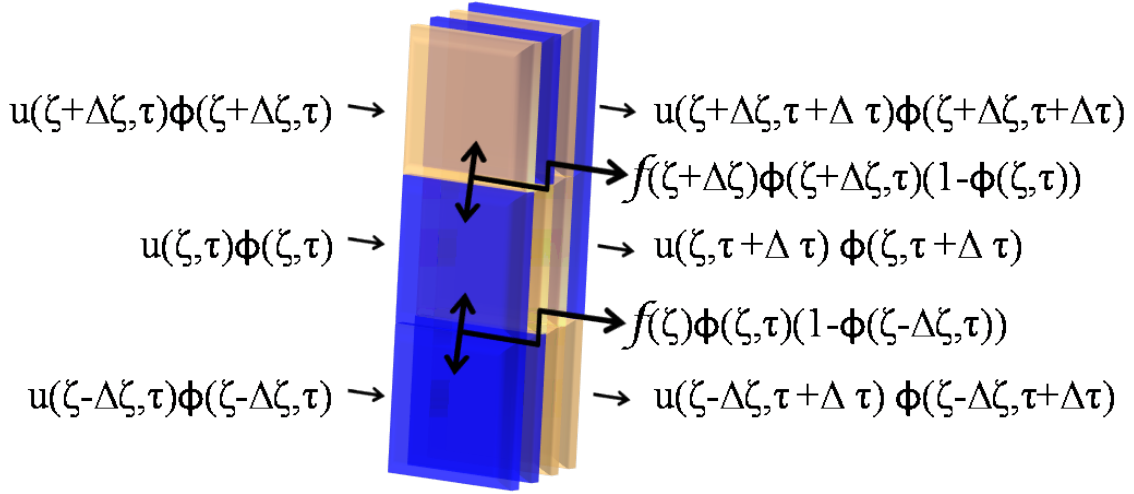


FIGURE 4.15: Fluxes of small concentration at a node, including contributions due to varying downslope velocity with height. We use this model to define our final analytic theory.

$$u \frac{\partial \phi}{\partial \tau} = \frac{\partial (k \frac{du}{d\zeta} \phi (1 - \phi))}{\partial \zeta}$$

We propose this as our final analytic theory to model particle size segregation.

## 4.2.2 Results

Comparison of the analytic and cellular automata simulation has turned out to be difficult because of the known shocks forming in the solution. Attempts have been made to both analytically and computationally solve the continuum model. Analytically, the method of characteristics has been employed to find a characteristic solution for the simple shear case, as shown above in Figure 4.14. We have solved numerically for the shear band regime, as we know that this should not exhibit any shock formation at the beginning of the flow. Only after approximately 90% of the segregation has occurred do we expect the discontinuity to break the numerical solution of the analytic model.

Because we always expect a discontinuity in the steady state solution, we know a priori that most numerical methods will fail. A finite difference solver has been used to describe the shear band flow case until a discontinuity in the solution is reached. This is pictured below in Figure 4.16, and compared with the cellular automaton solution for the same time and initial conditions. The results agree within 5%, up to the point at which a discontinuity is formed. From then on, the numerical method for solving

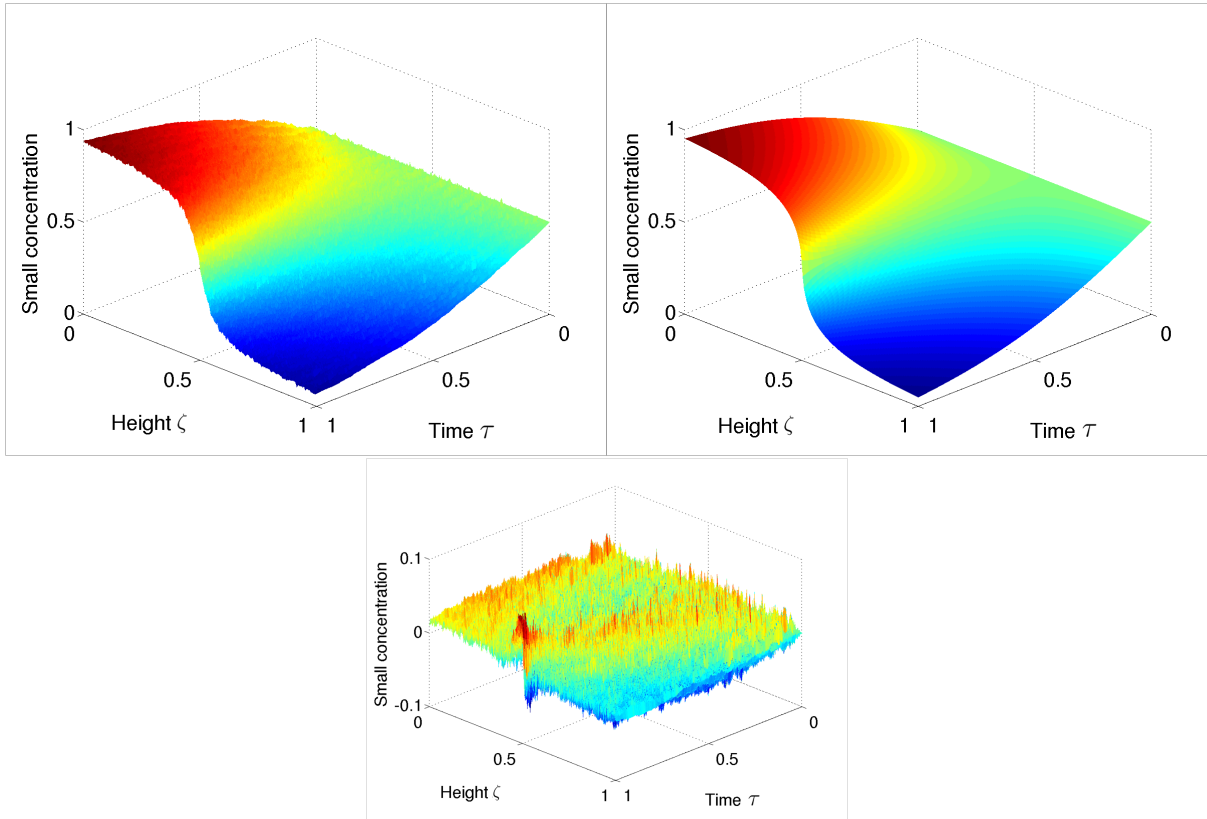


FIGURE 4.16: Comparison of cellular automaton and continuum approaches with same initial conditions  $\phi_0 = 0.5$  and  $f = \zeta(1 - \zeta)$ . Left: Cellular automaton. Right: Continuum approximation using a numerical solver. Bottom: Difference between two top plots. Note that the statistically based cellular automaton is rough, while the exact solution from the analytic model is smooth.

the analytic theory fails. A shock capturing method must be employed to accurately model the analytic solution, but this was beyond the scope of this thesis work.

The two simulations above vary not only because of the statistical nature of the cellular automaton. An important difference is that located at  $(\zeta = \frac{1}{2}, \tau = 1)$ , where the concentration shock begins. The finite difference model used to compute the solutions to the analytic equation fails entirely at discontinuities in the solution space, and so cannot be relied upon for this system.

## Summary of Results

---

### 5.1 Cellular automata

Our model predicts that in a physical flow, such as that approximated by Bagnold shear, a concentration shock develops at the bottom of the flow only. The appearance of a shock at the top of the flow is a result of the small number of particles being observed. Flow near the free surface in Bagnold shear can be approximated by plug flow, corresponding to a situation with extremely slow segregation. This supports our predictions in distinction from the previous two theories.

The time for segregation has been shown to be a function not only of the shear regime, but also the particle size. Interestingly, and in contrast to previous theory, the bigger particles percolate faster than the smaller particles. While one may at first postulate that particles would trickle through the bulk faster than others could be leveraged over them, this has been shown to be false.

### 5.2 Analytic model

The cellular automata lead directly to a continuum theory which described the model. This has been compared to existing theories and shown to be substantially superior. The mathematics is derived in an intuitive and easily reproducible form, allowing for a more complete understanding of the meaning of the governing equation. This advective partial differential equation has been solved using the method of characteristics and numerical finite differencing methods.

## Conclusion

---

Beginning with the simple idea that segregation in 1 dimension is the swapping of particles, we have devised both a cellular automata and a continuum mechanics approach which are more physical representations of kinetic sieving than those previously obtained.

It has been shown here that the previous work in this field can be consolidated into a cohesive, simple theory which contains the essence of both works. Just as the previous works were both empirically fitted, our single fitting parameter can adequately reproduce works obtained with either method.

We note that a dissociation exists between two levels of reality in the system. The pattern forming behaviour can be explained in terms of the percolation frequency, with quite little known about the structure or interaction of the particles, but the percolation frequency itself must be explained in another way. This has been done, for example, by Savage and Lun using a maximum entropy approach.

We have shown that in fact large particles segregate faster than slow particles, in sharp distinction from previous theory. This effect is due to the interaction of the shear stress with particle percolation velocities.

Starting with a very simple cellular automata, it has been shown that previously rigorously derived results can be explained without the analytic effort. By measuring the happiness of the particles, their likelihood of moving is found. For these particles, just as with humans, they are happiest with their own kind. Happy rocks stay, unhappy rocks leave and the big ones leave faster than the small ones.

## References

- I.S. Aranson and L.S. Tsimring. 2005. Patterns and collective behavior in granular media: Theoretical concepts. *Arxiv preprint cond-mat/0507419*.
- J.P. Bouchard, M. Cates, R. Pranash, and S.F. Edwards. 1994. A model for the dynamics of sandpile surfaces. *J. Phys. I France*, 4.
- T. Bouteux and PG De Gennes. 1996. Surface flows of granular mixtures: I. General principles and minimal model. *J. Phys. I France*, 6:1295–1304.
- J. Bridgwater and N. D. Ingram. 1971. Rate of spontaneous inter-particle percolation. *Chemical Engineering Research and Design*, 49a:163–169.
- D. Brone and FJ Muzzio. 1997. Size segregation in vibrated granular systems: A reversible process. *Physical Review E*, 56(1):1059–1063.
- Bastien Chopard and Michel Droz. 1998. *Cellular Automata Modeling of Physical Systems*. Cambridge Univ Press.
- WAV Clark. 1991. Residential preferences and neighborhood racial segregation: A test of the Schelling segregation model. *Demography*, pages 1–19.
- P.W. Cleary, G. Metcalfe, and K. Liffman. 1998. How well do discrete element granular flow models capture the essentials of mixing processes? *Applied Mathematical Modelling*, 22(12):995–1008.
- E. Clement, J. Rajchenbach, and J. Duran. 1995. Mixing of a granular material in a bidimensional rotating drum. *Europhysics Letters*, 30(1):7–12.
- VN Dolgunin, AN Kudy, and AA Ukolov. 1998. Development of the model of segregation of particles undergoing granular flow down an inclined chute. *Powder technology*, 96(3):211–218.
- M.B. Donald and B. Roseman. 1962. Mixing and demixing of solid particles. part 1. mechanisms in a horizontal drum mixer. *British Chem. Eng.*
- J.A. Drahn and J Bridgwater. 1983. The mechanisms of free surface segregation. *Powder Technology*, 36(1):39.
- J. Duran and R. Jullien. 1998. Attractive Forces in a Granular Cocktail. *Physical Review Letters*, 80(16):3547–3550.
- J. Gray and K. Hutter. 1997. Pattern formation in granular avalanches. *Continuum Mechanics and Thermodynamics*, 9(6):341–345.

- J. Gray and AR Thornton. 2005. A theory for particle size segregation in shallow granular free-surface flows. *Proceedings of the Royal Society A: Mathematical, Physical and Engineering Sciences*, 461(2057):1447–1473.
- H Henein, J.K. Brimacombe, and A.P. Watkinson. 1983. Experimental study of transverse bed motion in rotary kilns. *Metallurgical Transactions B*, 14:191–205, Jun.
- KM Hill, A. Caprihan, and J. Kakalios. 1997. Bulk segregation in rotated granular material measured by magnetic resonance imaging. *Physical Review Letters*, 78(1):50–53.
- BPB Hoomans, JAM Kuipers, and WPM Van Swaaij. 2000. Granular dynamics simulation of segregation phenomena in bubbling gas-fluidised beds. *Powder Technology*, 109(1-3):41–48.
- DA Huerta and JC Ruiz-Suarez. 2004. Vibration-induced granular segregation: a phenomenon driven by three mechanisms. *Arxiv preprint cond-mat/0402256*.
- N. Jain, J.M. Ottino, and R.M. Lueptow. 2005. Combined size and density segregation and mixing in noncircular tumblers. *PHYSICAL REVIEW E Phys Rev E*, 71:051301.
- DV Khakhar, JJ McCarthy, and JM Ottino. 1997. Radial segregation of granular mixtures in rotating cylinders. *Physics of Fluids*, 9:3600.
- DV Khakhar, JJ McCarthy, JF Gilchrist, and JM Ottino. 1999a. Chaotic mixing of granular materials in two-dimensional tumbling mixers. *Chaos: An Interdisciplinary Journal of Nonlinear Science*, 9:195.
- DV Khakhar, JJ McCarthy, and JM Ottino. 1999b. Mixing and segregation of granular materials in chute flows. *Chaos: An Interdisciplinary Journal of Nonlinear Science*, 9:594.
- R. Khosropour, J. Zirinsky, HK Pak, and RP Behringer. 1982. Convection and size segregation in a Couette flow of granular material. *Chem. Eng. Sci Phys Rev E*, 56:4467.
- JB Knight, HM Jaeger, and SR Nagel. 1993. Vibration-induced size separation in granular media: The convection connection. *Physical review letters*, 70(24):3728–3731.
- J.P. Koeppe, M. Enz, and J. Kakalios. 1998. Phase diagram for avalanche stratification of granular media. *Physical Review E*, 58(4):4104–4107, October.
- H.A. Makse. 1997. Stratification instability in granular flows. *Physical Review E*, 56(6):7008–7016.
- H.A. Makse. 1999. Continuous avalanche segregation of granular mixtures in thin rotating drums. *Physical Review Letters*, 83(16):3186–3189.
- G. Metcalfe and M. Shattuck. 1996. Pattern formation during mixing and segregation of flowing granular materials. *Physica. A*, 233(3-4):709–717.
- GDR MiDi. 2004. On dense granular flows. *The European Physical Journal E: Soft Matter and Biological Physics*, 14(4):341–365.
- M. Nakagawa, SA Altobelli, A. Caprihan, E. Fukushima, and E.K. Jeong. 1993. Non-invasive measurements of granular flows by magnetic resonance imaging. *Experiments in Fluids*, 16(1):54–60.

- N. Nityanand, B. Manley, and H. Henein. 1986. An analysis of radial segregation for different sized spherical solids in rotary cylinders. *Metallurgical Transactions B*, 17B(257), June.
- JM Ottino and DV Khakhar. 2000. Mixing and segregation of granular materials. *Annual Review of Fluid Mechanics*, 32(1):55–91.
- P.G. Rognon, J.N. Roux, M. Naaim, and F. Chevoir. 2007. Dense flows of bidisperse assemblies of disks down an inclined plane. *Physics of Fluids*, 19.
- A. Rosato, F. Prinz, KJ Standburg, and R. Swendsen. 1986. Monte Carlo simulation of particulate matter segregation. *Powder technology*, 49(1):59–69.
- A.D. Rosato, D.L. Blackmore, N. Zhang, and Y. Lan. 2002. A perspective on vibration-induced size segregation of granular materials. *Chemical Engineering Science*, 57(2):265–275.
- SB Savage and CKK Lun. 1988. Particle size segregation in inclined chute flow of dry cohesionless granular solids. *Journal of Fluid Mechanics*, 189:311–335.
- S.B Savage and J.W. Vallance. 2000. Particle segregation in granular flows down chutes. In *Iutam Symposium on Segregation in Granular Flows: Proceedings of the IUTAM Symposium Held in Cape May, NJ, USA, June 5-10, 1999*, page 31. Kluwer Academic Pub.
- SB Savage. 1987. Interparticle percolation and segregation in granular materials: A review. In *Developments in Engineering Mechanics: Proceedings of the Technical Sessions on Developments in Engineering Mechanics Held at the Canadian Society for Civil Engineering Centennial Conference, Montreal, Quebec, Canada, May 18-22, 1987*, page 347. Elsevier.
- Thomas C. Schelling. 1969. Models of segregation. *The American Economic Review*, 59(2).
- L. E. Silbert, D. Ertas, G. S. Grest, T. C. Halsey, D. Levine, and S. J. Plimpton. 2001. Granular flow down an inclined plane: Bagnold scaling and rheology. *Physical Review E*, 64(5), October.
- Arne Traulsen and Jens Christian Claussen. 2004. Similarity based cooperation and spatial segregation. *Physical Review E*, 70:046128.
- L. Trujillo, M. Alam, and H.J. Herrmann. 2003. Segregation in a fluidized binary granular mixture: Competition between buoyancy and geometric forces. *Europhysics Letters*, 64(2):190–196.
- R.A. Wilkinson, R.P. Behringer, J.T. Jenkins, and M. Louge. 2005. Granular materials and the risks they pose for success on the moon and mars. *NASA Publication*.
- Stephen Wolfram. 1986. Theory and applications of cellular automata. *Advanced Series on Complex Systems, Singapore: World Scientific Publication*.
- T. Yanagita. 1999. Three-dimensional cellular automaton model of segregation of granular materials in a rotating cylinder. *Physical Review Letters*, 82(17):3488–3491.

## Cellular automata MATLAB© script

```

%%%%%%%%%%%%%%%%%%%%%%%%%%%%%%%%%%%%%%%%%%%%%%%%%%%%%%%%%%%%%%%%%%%%%%%%
%%%%%%%%%%%%%%%%%%%%%%%%%%%%%%%%%%%%%%%%%%%%%%%%%%%%%%%%%%%%%%%%%%%%%%%%
CA - Lagrangian system for segregation %%%%%%%%%
%%%%%%%%%%%%%%%%%%%%%%%%%%%%%%%%%%%%%%%%%%%%%%%%%%%%%%%%%%%%%%%%%%%%%%%%
%%%%%%%%%%%%%%%%%%%%%%%%%%%%%%%%%%%%%%%%%%%%%%%%%%%%%%%%%%%%%%%%%%%%%%%%
25/09/09 %%%%%%%%%
%%%%%%%%%%%%%%%%%%%%%%%%%%%%%%%%%%%%%%%%%%%%%%%%%%%%%%%%%%%%%%%%%%%%%%%%

```

```

function CA
clear all
global A
lx=2000; % length (into page)
ly=lx/10; % height
for prob=[0.5]; % probability of segregation occuring, k
for small=[0.1:0.1:0.9]; % proportion of small
for flow=[0]; % shear condition parameter
t_c=2*ly/prob;
if flow==0 % simple shear
    V=prob*ones(ly,1);
    t_max=1.5*t_c;
elseif flow==1 % silbert shear profile vector
    V=prob*(1-linspace(0,1,ly))'.^0.5;
    t_max=3*t_c;
elseif flow==2 % linear shear
    V=prob*(1-linspace(0,1,ly))';
    t_max=2.5*t_c;
elseif flow==3 % shear band
    V=prob*(linspace(0,1,ly)'-linspace(0,1,ly)'.^2);
    t_max=2.5*t_c;
elseif flow==4 % PLUG FLOW
    V=prob*linspace(0,0,ly);
    t_max=5;
end

```

```
A=zeros(t_max,ly);

fprintf('%%%%%%%%% SIMULATION STARTING %%%%%%%%%%\n')
fprintf('ly=%d, lx=%d, t_max=%d, flow=%d\n',ly,lx,t_max,flow)
fprintf('p=%d, prob=%0.1f, small=%0.2f\n',p,prob,small)

%% BUILD WORLD %%

fprintf('Building world... ')
tic
s = sudoku(ly,lx,10,10,small); % using patch size of 10 for speed
A(1,:)=sum(s,2)/lx;
T=toc;
fprintf('World built in %2.2fmin\n', T/60)
fprintf('Starting time marching\n')
load('MyColormaps','mycmap')
T=0; tic

%% MAIN LOOP %%

for time=1:t_max
    a=mod(time,2); % odd/even time counter

    d_cr=build_d_cr(s,lx,ly); % Build d_cr

    for x=1:lx
        if mod(x,2)+a==1 % alternate between cases
            for y=2:2:ly-1 % case 1
                if rand(1)<V(y)
                    s=swap(s,d_cr,y,x,time);
                end
            end
        end
    end
end
```

```

        end
    else
        for y=3:2:ly-1 % case 2
            if rand(1)<V(y)
                s=swap(s,d_cr,y,x,time);
            end
        end
    end
end
end

end

%% OUTPUT %%

A(time+1,:)=sum(s,2)/lx;
if rem(time,t_max/10)==0
    T=T+toc;
    tic;
    fprintf('Progress: %3.0f%% Elapsed time: %3.0fmin Remaining...
time: %3.0fmin\n', time*100/t_max,T/60,T/60*(t_max/time-1))
end

end

figure(1)
set(1,'Colormap',mycmap)
axes('fontsize',30);
contourf(linspace(0,t_max/t_c,t_max+1), linspace(0,1,ly-1), ...
A(:,1:end-1),'LineStyle','none')%, colormap('gray')%, axis off
caxis([0 1]);
tt=sprintf('tmax_%d_p_%d_Prob_%.2f_small_%.2f_flow_%.2f_up.png',...
t_max, p, prob, small, flow);
print ('-dpng', tt)

% PRINT TXT FILE OUTPUT

```

```

tt=sprintf('tmax_%d_p_%d_Prob_%.2f_small_%.2f_flow_%.2f_up.txt',...
t_max, p, prob, small, flow);
csvwrite(tt,A')

fprintf('%%%%%%%% SIMULATION FINISHED %%%%%%%%%\n')
end
end
end
end

function s=swap(s,d_cr,y,x,time)
    if s(y,x)>s(y-1,x) % SWAP WITH BELOW IF SMALL
        tt=s(y,x);
        s(y,x)=s(y-1,x);
        s(y-1,x)=tt;
    end
end

function d_cr=build_d_cr(s,lx,ly)
d=sign(max(0,s)); % denominator to divide by
% AVERAGE THROUGH LENGTH
d_cr=zeros(ly,lx);
    for x=1:lx
        d_cr(:,x)=sum(s,2)/lx;
    end
end

function T = sudoku(ly,lx,patchy,patchx,phi0)
S=[]; M = zeros(patchy,patchx);% time=0;
M_new = zeros(patchy,patchx); count=0;
fprintf('Number of patches to create: %3.0f ...
\n', (ly*lx)/(patchy*patchx))

```

```

while size(S,3)<(ly*lx)/(patchy*patchx) % to stitch together
    while sum(sum(M))<phi0*patchy*patchx
        if M==M_new
            count=count+1;
        else
            count=0;
        end
        if count==patchy*patchx % IF THAT FAILED, TRY AGAIN
            M_new=zeros(patchy,patchx);
        end
        M=M_new;
        i=randi(patchy,1);
        j=randi(patchx,1);
        if sum(M(i,:))<phi0*patchx && sum(M(:,j))<phi0*patchy
            M_new(i,j)=1;
        end
    end
    S=cat(3,S,M);
    M = zeros(patchy,patchx); M_new = zeros(patchy,patchx); count=0;
end
T=zeros(ly,lx);
for i=1:ly/patchy
    for j=1:lx/patchx
        T(1+patchy*(i-1):patchy*i,1+patchx*(j-1):patchx*j) = ...
        S(:, :, i+j*(ly/patchy-1));
    end
end
end
end

```